Paulo Roberto de Castro Mendes Junior

Free Surface Flows with Complex Interfaces

Dissertação de Mestrado

Dissertation presented to the Programa de Pós-Graduação em Engenharia Mecânica of PUC-Rio in partial fulfillment of the requirements for the degree of Mestre em Engenharia Mecânica.

Advisor: Prof. Márcio da Silveira Carvalho

Rio de Janeiro
May 2019

PONTIFÍCIA UNIVERSIDADE CATÓLICA
DO RIO DE JANEIRO

Paulo Roberto de Castro Mendes Junior

Free Surface Flows with Complex Interfaces

Dissertation presented to the Programa de Pós-Graduação em Engenharia Mecânica of PUC-Rio in partial fulfillment of the requirements for the degree of Mestre em Engenharia Mecânica. Approved by the undersigned Examination Committee.

Prof. Márcio da Silveira Carvalho
Advisor
Departamento de Engenharia Mecânica – PUC-Rio

Prof. Paulo Roberto de Souza Mendes
Departamento de Engenharia Mecânica – PUC-Rio

Prof. Angela Ourivio Nieckele
Departamento de Engenharia Mecânica – PUC-Rio

Rio de Janeiro, May 15th, 2019

Paulo Roberto de Castro Mendes Junior

Bachelor in Engenharia Mecânica by Pontifícia Universidade Católica do Rio de Janeiro (2016)

To my family for their love and support.

Acknowledgments

In my earliest memories, my family is present. By they, I was loved, supported and taught. I learned about character, right and wrong in practice, following their example. When I learned to take my first steps, my family was present. Raising me when I fall. Even today, I feel that in any falling, they will still be around to help me get up. I owe everything to my family.

When I needed to take a few steps alone, I found people who made my journey more interesting. With them, I shared moments of joys, sadness, victories, and difficulties. Today, seeing them older and successful, I am touched by today to call them friends.

During my graduation at PUC-RIO, I was fortunate to join the LMMP group. What I suppose a milestone in my education and a great stimulus to recover hope and keep dreaming. Here, contributing to this high-performance group I had matured professionally and personally. Thank you, Professor Marcio and Frederico, for this incredible opportunity. Thank you, lab colleagues, for the company and teachings.

Abstract

de Castro Mendes Junior, Paulo Roberto; da Silveira Carvalho, Márcio (Advisor). **Free Surface Flows with Complex Interfaces**. Rio de Janeiro, 2019. 66p. Dissertação de Mestrado – Departamento de Engenharia Mecânica, Pontifícia Universidade Católica do Rio de Janeiro.

Several processes present free surfaces flows. Some of those processes go beyond engineering problems, including everyday issues like raindrops falling from the sky, water flowing down the river or through a faucet. In industry, extrusion and coating process are two examples of processes that are strongly affected by the behavior of the interface. The most commonly used free interface model was developed in the 19th century and describes as isotropic the behavior of interfaces and dependent on a single parameter called interfacial tension. Since then, advances in the area of interfacial rheology have been showing that the interfacial phenomena are more complex and accurate of more information to be modeled. In this line of thinking, this work analyzes the effect of interface viscosity on the dynamics of extrusion and slot coating process, in which the set of differential equations that governs the problem is solved by Finite Element method.

Keywords

Resumo

de Castro Mendes Junior, Paulo Roberto; da Silveira Carvalho, Márcio. **Escoamentos de Superfícies Livre com Interface Complexas**. Rio de Janeiro, 2019. 66p. Dissertação de Mestrado – Departamento de Engenharia Mecânica, Pontifícia Universidade Católica do Rio de Janeiro.

Diversos processos apresentam escoamentos com superfícies livres. Alguns desses processos vão além dos problemas de engenharia, incluindo questões cotidianas como gotas de chuva caindo do céu, água fluindo pelo rio ou através de uma torneira. Na indústria, o processo de extrusão e revestimento são dois exemplos de processos que são fortemente afetados pelo comportamento da interface. O modelo de interface livre mais comumente utilizado foi desenvolvido no século XIX e descreve como isotrópico o comportamento das interfaces e dependente de um único parâmetro, denominado tensão interfacial. Desde então, os avanços na área de reologia interfacial vêm mostrando que os fenômenos interfaciais são mais complexos e precisam de mais informações para serem modelados. Nesta linha de pensamento, este trabalho analisa o efeito da viscosidade interfacial na dinâmica do processo de extrusão e revestimento por slot, no qual o conjunto de equações diferenciais que governam o problema é resolvido pelo método dos elementos finitos.

Palavras-chave

Extrusão de Fluido; Revestimento em Slot Die; Interfaces Complexas; Viscosidades interfaciais.

Table of contents

List of figures

List of tables

List of Abreviations

Greek Symbols

ρ - Density

μ - Viscosity for Newtonian fluid

μ_Γ - Extensional viscosity for fluid surface

λ_Γ - Dilatational viscosity for fluid surface

σ - Surface tension

σ_Γ - Boussinesq surface stress tensor

$\nabla_\Gamma \cdot \boldsymbol{u}$ - Divergent of velocity along the surface

$\nabla_\Gamma \cdot \boldsymbol{\sigma}_\Gamma$ - Divergent of Boussinesq surface stress tensor along the surface

Roman Symbols

Ca - Capillarity number

Bq - Boussinesq number

*"Even paradise could become a prison if one
had enough time to take notice of the walls."*

Morgan Rhodes .

1
Introduction

1.1
Motivation

Several processes present free surfaces flows. Some of those processes go beyond engineering problems, including everyday situations like raindrops falling from the sky, water flowing down the river or through a faucet.

Extrusion and slot die coating are examples of industrial material processing in which the free surface flow is key in the process success. Extrusion is the forced passage of material through an orifice (or die) [1]. The material shape conforms to the die's design. The continuous fluid supply allows the fabrication of long objects with constant and complex cross-sections and excellent accuracy. Copper wires, aluminum bars and even several food doughs are products of extrusion processes. In the extrusion of fluids, typically, a single screw is responsible for driving the fluid from the feed hopper to the exit orifice.(see Figure 1.1)

Figure 1.1: Representation of an extrusion flow.

There is no unique extruder design, so that both the diameter and pitch of the screw and the channel diameter can vary throughout the apparatus. The design will depend on the materials' properties and the rate of production. But in all of them, the rotation speed of the screw defines the flow rate [2].

The extrusion process frequently deals with a swelling of the fluid after exiting the die. This phenomenon called Die Swell, Extrudate Swell or Baurus effect and is evident for some non-Newtonian fluids but also occur at a smaller scale for Newtonian liquids [2, 3, 4]. Long molecule chains are oriented and uncoiled as they exit the die in the extensional dominated flow. Compressive

normal stresses leads to an expansion of the flow. The flow inside the extruder assumes the parabolic velocity profile which becomes uniform after leaving the cavity. This profile transition decelerates the fluid and leads to an increase in the thickness of the extrudate. The intensity of the swell depends on the flow rate, cross-section dimensions, and fluid properties. Modifications in the extrusion operation parameters may change the final diameter of the extrudate. The Die-swell predictions help in the design of the die as well as in the evaluation of the energy required for the process.

Another example of manufacturing free surface flow is slot coating flow. The slot die coating is a process that covers a substrate moving at high speed with a thin layer of fluid. The apparatus is composed of two metal structures called lips. When placed together these lips create a narrow channel which guides the fluid to the substrate. An elongated chamber between the lips supports the uniform profile flow rate at the exit of the channel (Figure 1.2).

As the die does not touch the substrate, air and fluid fill the gap between these components. Two menisci separate the air from the coating liquid and the region between this menisci is called coating bead. The quality of the coated film is directly affected by the stability of the flow in the coating bead. A slight vacuum applied at the upstream meniscus enables coating very thin films [5, 6, 7, 8, 9, 10].

Figure 1.2: Representation of a slot-die coating flow.

Far from the die, the fluid moves in plug flow with the substrate velocity. The thickness of the liquid layer is set by the imposed flow rate and the velocity of the moving substrate. As both are independent of other process variables, slot coating belongs to a class of coating methods known as pre-metered coating and being ideal for high precision processes used in the production of adhesive, magnetic tapes, specialty papers, imaging films, and many other products.

The primary coating variables are the die geometry, the flow rate, the speed of the substrate and the vacuum pressure. For a given material there is normally an envelope of process conditions which leads to smooth coating. These condition ranges are known as operating window [6, 5]. Knowledge of the coating window allows predicting whether a particular method can be used to coat a given substrate at a prescribed production rate.

Interface rheology is a key concept to model a free surface flow. The most common hypothesis used for free surfaces flows treats interfacial behavior as a simple interface. The traction acting along the simple interface is isotropic and constant. Its value is proportional to a property associated with the pair of fluids that forms the interface, called interfacial tension. The hypothesis that an unique property describes the mechanical behavior of a liquid-liquid interface is valid in many situations. However, in flows involving solutions of polymer surfactants and others complex interface acting materials, the interface behavior can be complex. Recent studies on complex interfaces have shown that they can exhibits viscous and elastic behavior. The traction along the interface can become non-isotropic and be a function of the surface deformation and rate of deformation.

The effect of interface rheology is usually not taken into account on the analysis of free surface flows. Interface rheology may have a strong impact on the flows behavior and consequently on extrusion and slot coating flows. This work addresses this problem.

1.2
Literature Review

The first model of an interface is also the simplest model. The Young-Laplace equation comes from the hypothesis that the traction along the interface is isotropic and proportional to the interfacial tension between the two liquid phases. A direct consequence is that there is pressure difference between the two phases equal to the interfacial tension times the interface curvature. This model works very well for pure fluid surfaces and explains the capillary action that causes fluids to move against atmospheric pressure in capillary tubes. An important dimensionless parameter in free surface flow is the capillary number, which represents the ratio between viscous to interfacial forces, defined as:

$$Ca = \frac{\text{viscous drag forces}}{\text{surface tension forces}} = \frac{\mu V}{\sigma}, \qquad (1\text{-}1)$$

where μ represents the fluid viscosity, V represents a characteristic velocity and σ represents the surface tension. Therefore, Young-Laplace interfacial model assumes that the interface does not depend on either the history of deformation or the rate of deformation, which makes this model too simple to represent interface populated by particles, long molecules or other complex surface active compounds.

The surfactants, for example, are substances that usually reduce the

surface tension. The surface-active agents or surfactant is an amphipathic structure consisting of a lyophobic part that has an "affinity for solvent" and a lyophobic part with an "aversion to solvent" [11]. At low concentration, when the molecules do not interact with each other, the surfactants orient themselves forming a monomolecular layer at the interface that decreases the attraction between the molecules of the surface. The lower cohesion between the interfacial molecules decreases the energy to create new areas. Therefore, the surface tension decreases. Still considering the low amount of solvents adsorbed to the surface, more molecules on the surface means less surface tension. However, the free surface is subject to expansions and contractions during a flow. Gibbs published in 1878 a relationship between the changes in concentration of a molecules in contact with a surface and the changes in the surface tension This equation takes into account the area of the surface [12]. So, even for a constant number of molecules, the concentration of surfactants can change because the distribution of molecules respond to the surface motion. So a single value of the surface tension is no more sufficient to describe the interface behavior because it is at least a function of concentration.

The physicochemical Hydrodynamics couples the interface and the bulk in a nonlinear dynamics that can lead to regions of non-homogeneous molecules inducing a displacement of fluid trying to balance the gradient of molecule concentration. Marangoni explained this phenomenon, which received his name [13]. The molecule-poor region has a higher surface tension than the rich molecule region. This difference of tensions induces a net force that spread out the molecules at the high concentration region reducing molecular concentration while compressing the low concentration region increasing the molecular concentration. That is the case of Lower molecular weight (LMW) surfactants. Sternling and Scriven have shown the importance of molecular concentration on the stabilization of liquid phases in contact with a plane interface. When a drop of clean fluid is carefully placed on the surface of another molecule-populated fluid or vice versa, a disturbance to the surface arises. The researchers were able to explain the appearance of these perturbation based on the Marangoni effect.

The interaction between the molecules and the interface strongly depends on the type of molecules adsorbed on it. The LMW surfactants have a small size and do not self-assemble into complex microstructures [14]. LMW surfactants usually lower the surface tension more than the bigger molecules, but proteins adsorb better on the surface [15]. The proteins are macromolecules and surface-active compounds of long polymer chains. Both types of molecules stabilize the surface in which they are adsorbed. LMW surfactants induce the Marangoni

displacement by lowering surface tension. Although the proteins also decrease the surface tension, its stabilization mechanism is due to the formation of a viscoelastic monolayer on the interface [16].

The non-linear response to the deformations are characteristics of complex rheological interfaces (or complex interfaces). Complex interfaces are familiar to live systems, foods and the environment. This rheological characteristic is essential to such bio-process as the ones that occur in the lung and biological membranes [17, 18].

Recently, Shirazi *et al.* [19] have used the pendant drop method to characterize the interface mechanical behavior of a Laponite based Pickering films of the oil drop in water. Laponite is a synthetic smectite clay composed of monodisperse thick disks. The laponite layer behavior changes in the presence of salt due to molecular interactions. The salt increases the maximum concentration of laponite at the interface of the drop and with that increases the elasticity and viscosity moduli. In their experiments, the effect of aging time increased the elastic modulus up to approximately 600 mN/m a suspension of 1.5 wt% of Laponite in 0.1 M NaCl.

Shirazi *et al.* [20], shown in another study the impact of this behavior on the Laponite stabilization of the oil-water emulsion. Oil drops coalescence did not occur and the solution remained stable during more than one month in the salty medium.

Rosenfeld and Fuller[21] and Bhamla *et al.* [22], motivated by the stability of the tear film in the eye, have compared the impact of the insoluble layer characteristics on the dewetting time of a silicon wafer. They explored a mix of wax esters, cholesterol esters, and fatty acids called meibum that covers our eyes with a film of proteins and mucins. This mix of molecules performs significant biological roles. Patients with these lipid deficiencies suffer from early dryness of the tear film leading to irritations and inflammation in the cornea. The study focused on the effect of three insoluble surfactants with different interfacial rheological properties. They have shown that meibum with viscoelastic properties, in which the elastic modulus exceeds the viscous modulus, expressively increased the dewetting time in comparison with a viscoelastic monolayer with high viscous modulus and a viscous interface.

Complex interfacial become relevant in systems with large interfacial areas. Boussinesq was the first to propose the necessity of taking into count the length scale [17, 18]. The Boussinesq number is a dimensionless group that couples the surface shear stress, the bulk stress and the length scale evaluating

the importance of the surface on the flow [23].

$$Bq = \frac{\text{surface shear viscosity}}{\text{bulk viscosity} \times \text{length scale}} = \frac{\mu_\Gamma}{\mu L} \qquad (1\text{-}2)$$

Here μ_Γ represents the surface shear viscosity, μ represents the bulk shear viscosity and L a characteristic length. This phenomenon has also be studied by others researches. Scriven rewrote Boussinesq's equations in terms of an arbitrary moving surface and deforming coordinate system in a more convenient mathematical model [18, 24]. The Boussinesq-Scriven law is forces balance on the surface write in tensor form, which takes into account not only the shear viscosity but also the dilatational viscosity on the surface.

The shear viscosity, as well as the dilatation viscosity, are properties that respond to the velocity gradients and can have a significant effect on the flow behavior strongly influencing the dynamics of the surface. The shear viscosity is that viscosity measured at a constant area. The dilatational viscosity is measured compressing or dilatating the volume but keeping the original shape.

This dynamic property has a substantial impact on thin films as extrusion of fluid and slot-die coating, and it has received little attention in the literature.

In addition to shear and dilatational interfacial deformation modes there are bending and torsion modes that are usually neglected. (For this and more information about deformation modes in complex interface consult [25, 26])

1.3
Objective

As described, isotropic interface models are widely used to describe free surface micro-flows. The objective of this work is to determine the effect of interface rheology on free surface flow dynamics. The working fluid was considered as Newtonian with a viscous interface. A Newtonian fluid was used, such that all atypical behavior can be attributed to the interfacial viscosity. This choice allows concentrating on the viscous interface instead of giving too much attention to the bulk phase.

This analysis was done numerically with finite element method and diffusion-like dynamic mesh, to solve the free boundary problem. The next section presents more discussions on the mathematical model used.

The solution obtained has enable to understand better the effect of interfacial viscosity on the extrusion of fluids and slot-die coating

2
Mathematical Formulation

This chapter presents the model that describes the free surface flows taking into account viscous behavior of liquid-gas interface. The model is used to study the effect of interface rheology on die-swell and slot coating flow.

Mass and the momentum conservation equations describe the flow. Both coating and extrusion operate in steady-state and at a constant temperature. So the liquid properties can be approximated as constant values.

2.1
Conservation Equations

The Navier-Stokes (NS) and the mass conservation equations govern the flow of a Newtonian fluid. NS arises from the Cauchy equation of motion that is the result of linear momentum conservation [27]. The Cauchy equation is a partial differential vector equation that describes the dynamics of any continuous media,

$$\rho \frac{D\boldsymbol{u}}{Dt} = \rho \boldsymbol{g} + \boldsymbol{\nabla} \cdot \boldsymbol{T}, \tag{2-1}$$

where ρ is the fluid density, $\boldsymbol{u}$ is the flow velocity, t is the time dependency and $\rho \boldsymbol{g}$ is the body force per unit of volume and $\boldsymbol{T}$ is the stress tensor. Equation 2-1 is a force balance where the left side represents the mass times acceleration of the fluid while the right side is a sum of the body and surface forces. For a Newtonian fluid, the stress tensor is:

$$\boldsymbol{T} = -p\boldsymbol{I} + \mu[\nabla \boldsymbol{u} + \nabla \boldsymbol{u}^T] - \frac{2}{3}\mu \nabla \cdot \boldsymbol{u}\,\boldsymbol{I}, \tag{2-2}$$

where μ is the viscosity of the fluid, $\boldsymbol{u}$ is the flow velocity and $\boldsymbol{p}$ is the fluid pressure. However, the system is still incomplete. The mass conservation complete the algebraic system,

$$\frac{\partial \rho}{\partial t} + \nabla \cdot (\rho \boldsymbol{u}) = 0. \tag{2-3}$$

The density is constant for a incompressible fluid. Mass conservation equation becomes:

$$\nabla \cdot \boldsymbol{u} = 0. \tag{2-4}$$

In steady state, the time dependency of $\boldsymbol{u}$ is zero, and the material derivative is equal to the convective term. In the absence of body forces, the eq 2-1 becomes:

$$\rho\, \boldsymbol{u} \cdot \nabla \boldsymbol{u} = -\boldsymbol{\nabla}p + \mu\nabla^2\boldsymbol{u}. \tag{2-5}$$

The section 2.2 presents the viscous interface model and section 2.3 the other boundary conditions.

2.2
Viscous Interface Modeling

The Boussinesq-Scriven constitutive Law describes viscous interface behaviour [28]. The surface stress is written as,

$$\boldsymbol{\sigma}_\Gamma = [\tau + (\lambda_\Gamma - \mu_\Gamma)\nabla_\Gamma \cdot \boldsymbol{u}]\boldsymbol{P} + \mu_\Gamma\boldsymbol{P}(\nabla_\Gamma\boldsymbol{u} + (\nabla_\Gamma\boldsymbol{u})^T)\boldsymbol{P}, \tag{2-6}$$

where τ is the interfacial tension and μ_Γ and λ_Γ are the the shear and dilatational interface viscosity. $\boldsymbol{P} = \boldsymbol{I} - \boldsymbol{n}\boldsymbol{n}^T$ is the projection tensor, with $\boldsymbol{n}$ being the local unit normal vector. $\nabla_\Gamma\boldsymbol{v} = P\nabla\boldsymbol{v}$ is the velocity gradient along the interface. $\nabla_\Gamma \cdot \boldsymbol{v} = tr(\nabla_\Gamma\boldsymbol{v})$ is the divergent along the interface.

Considering two dimensional flows, theses operators can be simplified by rewriting them as function of the surface unity tangent vector $\boldsymbol{t}$. Since $\boldsymbol{P} = \boldsymbol{t}\boldsymbol{t}^T$, it is possible to show that $\boldsymbol{P}\nabla_\Gamma\boldsymbol{v}\boldsymbol{P} = \boldsymbol{P}(\nabla_\Gamma\boldsymbol{v})^T\boldsymbol{P} = (\nabla_\Gamma \cdot \boldsymbol{v})\boldsymbol{P}$. So equation 2-6 becomes:

$$\boldsymbol{\sigma}_\Gamma = [\tau + (\lambda_\Gamma + \mu_\Gamma)\nabla_\Gamma \cdot \boldsymbol{u}]\boldsymbol{P} \tag{2-7}$$

If the interface viscosity is equal zero, the model recovers the isotropic interface model. In the case of liquid-gas interface, for gas pressure equal to p_g, force balance along the interface leads to:

$$\boldsymbol{n} \cdot \boldsymbol{T} = -p_g\boldsymbol{I} + \nabla_\Gamma \cdot \boldsymbol{\sigma}_\Gamma, \tag{2-8}$$

The effect of interface viscosity is noted on regions where the fluid is being deformed. Deformation occur where the interface points move at different speeds. The surface divergence of the velocity measures the interface deformation rate. If the velocity increases with the arc length, the interface expands or contracts if the speed is decreasing.

From the point of view of the arc length, the divergent along the interface becomes a simple derivative. Rewriting equation 2-8 in terms of the arc length allows a better understanding of the effect of interface viscosities on the forces along the meniscus.

$$\nabla_\Gamma \cdot \boldsymbol{\sigma}_\Gamma = \frac{d}{ds}\left[\left(\tau + (\lambda_\Gamma + \mu_\Gamma)\frac{d|u|}{ds}\right)\boldsymbol{t}\right] \tag{2-9}$$

$$\nabla_\Gamma \cdot \boldsymbol{\sigma}_\Gamma = \underbrace{\left(\frac{d\tau}{ds} + (\lambda_\Gamma + \mu_\Gamma)\frac{d^2|u|}{ds^2}\right)\boldsymbol{t}}_{\text{tangential direction}} + \underbrace{\left(\tau + (\lambda_\Gamma + \mu_\Gamma)\frac{d|u|}{ds}\right)\frac{d\boldsymbol{t}}{ds}}_{\text{normal direction}} \tag{2-10}$$

Eq 2-10 represents the tension force acting on the interface, and it has a normal and a tangential direction components. The normal component is proportional to the curvature and leads to the Young-Laplace equation, for a non-viscous interface. The additional term on the normal component is proportional to the interfacial viscosities and modifies the value of interfacial tension, which leads to "apparent interfacial tension". This apparent interfacial tension is a function of the variation of the module of the speed along the arc. If the interface decelerates along the arc, the apparent interfacial tension decreases. In this case, a mechanical process is responsible by the variance of the surface tension. On the tangential term, the derivative of the surface tension is zero when the concentration of surfactants is constant. Therefore, the additional term on the tangential component can induce the displacement of fluid, also for a constant concentration of surfactants hypothesis.

2.3
Boundary Conditions

2.3.1
Extrusion Flow

Figure 2.1 shows a sketch of the flow domain. Liquid flows between two parallel plates until reaching the end, from which a free surface is formed.

The shape of the free surface is unknown a priori and is a function of liquid properties and flow conditions.

Figure 2.1: Representation of the boundary conditions of extrusion flow.

This flow is symmetric, the set of equations is solved only in half of the domain. The physical domain is bounded by five boundaries listed below and displayed in Figure 2.1.

1 - Inlet: The flow at the entrance is assumed developed as consequence of the omitted part of the die. Fixing the flow rate Q, the velocity profile is:

$$\boldsymbol{u}(x=0,y) = \frac{3Q}{2H}\left(1-\frac{y^2}{H^2}\right)\boldsymbol{i} \qquad (2\text{-}11)$$

2 - Line of Symmetry: Absence of flux through this line and zero tangential force:

$$\boldsymbol{n}\cdot\boldsymbol{u} = 0 \; ; \; \boldsymbol{n}\cdot\boldsymbol{T}\cdot\boldsymbol{t} = 0 \qquad (2\text{-}12)$$

3 - Outlet: The outlet is not actually a physical boundary but just an artificial limit of domain. It must be far enough so the flow becomes well developed. The pressure is fixed and equal to p_g.

$$\boldsymbol{n}\cdot\nabla\boldsymbol{u} = 0 \qquad (2\text{-}13)$$

$$p = p_g \qquad (2\text{-}14)$$

4 - Free Surface:
Along the liquid-gas interface, two boundary conditions are imposed, there is no flux across the interface and the liquid traction must balance the interface force.

$$\boldsymbol{n} \cdot \boldsymbol{v} = 0 \tag{2-15}$$

$$\boldsymbol{n} \cdot \boldsymbol{T} = -p_g \boldsymbol{n} + \nabla_\Gamma \cdot \boldsymbol{\sigma}_\Gamma \tag{2-16}$$

5 - Fixed Wall: The top of the channel is a fixed wall which refers to the condition of non-slip and non-penetration.

$$\boldsymbol{u} = 0 \tag{2-17}$$

2.3.2
Slot Coating Flow

The complete simulation of this process should consider the entry from the fluid inlet to the region comprised between the two menisci. However simulation of the downstream is sufficient to determine the effect of the surface viscosity along the downstream meniscus, which is the objective of this analysis.

Figure 2.2: Representation of the boundary conditions on slot-die coating flow.

The physical domain is bounded by five boundaries listed below and displayed in Figure 2.2.

1 - Inlet: The inlet velocity profile now has to respect the velocity conditions at the extremes. $\boldsymbol{u}(x = 0, y = H) = 0$ and $\boldsymbol{u}(x = 0, y = 0) = V_S \boldsymbol{i}$ in addition to the known flow rate Q.

$$\boldsymbol{u}(x, y = 0) = \frac{6Q}{H}\left[\left(\frac{y}{H}\right) - \left(\frac{y}{H}\right)^2\right]\boldsymbol{i} \tag{2-18}$$

2 - Moving Wall: The flow on the bottom moves adhered to the wall respecting the condition of no-slip and no-penetration. So the condition is:

$$\boldsymbol{u}(x, y = 0) = V_S\boldsymbol{i} \tag{2-19}$$

3 - Outlet: The outlet is not actually a physical boundary but just an artificial limit of domain. It must be far enough so the flow becomes well developed. The pressure is fixed and equal to p_g.

$$\boldsymbol{n} \cdot \nabla\boldsymbol{u} = 0 \tag{2-20}$$

$$p = p_g \tag{2-21}$$

4 - Free Surface: Along the liquid air interface, two boundary conditions are imposed, there is no flux across the interface and the liquid traction must balance the interface force.

$$\boldsymbol{n} \cdot \boldsymbol{v} = 0 \tag{2-22}$$

$$\boldsymbol{n} \cdot \boldsymbol{T} = -p_g\boldsymbol{n} + \nabla_\Gamma \cdot \boldsymbol{\sigma}_\Gamma \tag{2-23}$$

5 - Fixed Wall: The top of the channel is a fixed wall which refers to the condition of non-slip and non-penetration.

$$\boldsymbol{u} = 0 \tag{2-24}$$

2.4
Dimensionless Groups

As the inertia can be neglected in both flows, the capillary and the Boussinesq numbers suffice to define the stokes problem.

2.4.1
Extrusion Flow

Using the inlet mean velocity as characteristic velocity that can be calculated as a function of the flow rate Q and the half cross-section height H. The capillary number assume the form:

$$Ca = \frac{\mu V}{\sigma} = \frac{\mu Q}{\sigma H} \qquad (2\text{-}25)$$

The Boussinesq number also uses the half height H as the length scale for the extrusion flow.

$$Bq = \frac{\mu_\Gamma}{\mu H} \qquad (2\text{-}26)$$

A dimensionless pressure was constructed using the bulk shear viscosity, the characteristic velocity and length.

$$P = \frac{\mu Q}{H^2} P_{Dimensionless} \qquad (2\text{-}27)$$

2.4.2
Slot Coating Flow

The capillary number can be calculated directly in function of the substrate velocity V_S.

$$Ca = \frac{\mu V_S}{\sigma} \qquad (2\text{-}28)$$

The Boussinesq number uses the coating gap as H the length scale for the slot coating flow. (Note that H represents the length scale for both problems. But it assumes different values for each flow.)

$$Bq = \frac{\mu_\Gamma}{\mu H} \qquad (2\text{-}29)$$

A dimensionless pressure was constructed using the bulk shear viscosity, the substrate velocity and coating gap.

$$P = \frac{\mu Q}{H^2} P_{Dimensionless} \qquad (2\text{-}30)$$

A dimensionless flow rate can be defined as the ratio between the feed flow rate and the flow rate required to coat a substrate with a film having a

thickness H. This is useful because the dimensionless flow rate is equal to the ratio between the thickness of the coated film and H.

$$\frac{Q}{V_S H} = \frac{\text{film thickness}}{H} \tag{2-31}$$

3
Numerical Solution

3.1
Finite Element Method

The Finite Element Method is based on the Weighted Residual Method that writes the approximate solution of a differential equation as a linear combination of continuous and differentiable functions. The method arises from the integral (weak or variational) form of the problem that transforms the linear combination of functions in a projection of the real solution on the subspace of these functions.

The attractiveness of Finite Element Method (FEM) lies on using basis functions that are different from zero in only a part of the domain, which allows describing the approximated solution in various geometries without additional difficulties. The FEM's robustness and efficiency made it famous in problems of modeling by differential equations such as fluid dynamics.

When the weighting functions used to calculate the residual of the equations are equal to the basis functions used to approximate the unknown fields, the FEM is known as Galerkin's Finite Element Method (GFEM). Just as in FEM, GFEM also generates a projection of the solution in the function space. Nevertheless, in the second case, this projection is orthogonal. The GFEM and some slight variations including numerical stabilizations techniques, such as the Streamline-Upwinding Petrov-Galerkin formulation, have been widely used to solve many problems in fluid mechanics in the last few years, including coating and free-surface flows of Newtonian and non-Newtonian liquids.

3.2
Mesh

The formulation described in the previous section is a free surface problem since the domain where the flow occurs is unknown. The position of the interfaces depends strongly on the velocity and pressure fields that depend on the interfacial position. To solve this problem, the system of differential equations and the boundary conditions formulated in the physical

domain will be transformed into an equivalent system defined in a reference or computational domain Ω_0. This transformation is done by mapping $\boldsymbol{x} = \boldsymbol{x}(\boldsymbol{\xi})$ (direct mapping) that connects the two domains ($\Omega_0 \rightarrow \Omega$). The physical domain is parameterized by the position vector $\boldsymbol{x} = (x, y)$ and the reference domain by $\boldsymbol{\xi} = (\xi, \eta)$ [29, 30].

To write the equations that govern the problem in the weak form, the derivatives with respect to the coordinates of the physical domain (x, y) must be represented by derivatives with respect to the coordinates of the reference domain (ξ, η). The Mapping Deformation Gradient Tensor is defined, in the $2D$ case as:

$$\nabla_\xi \boldsymbol{x} = \frac{\partial \boldsymbol{x}}{\partial \boldsymbol{\xi}} = \begin{pmatrix} \dfrac{\partial x}{\partial \xi} & \dfrac{\partial y}{\partial \xi} \\ \dfrac{\partial x}{\partial \eta} & \dfrac{\partial y}{\partial \eta} \end{pmatrix} \tag{3-1}$$

$\nabla_\xi \boldsymbol{x}$ is also the Jacobian matrix and its determinant must be different from zero to guarantee the transformation is invertible. Another restriction to the mapping the boundary of the computation domain on the boundary of the physical domain. With respect to this requirement, correction of the elemental area in the weak formulation integrals is allowed using $d\Omega = |\nabla_\xi \boldsymbol{x}|^{-1} d\Omega_0$. Moreover, any function α written according to the computational coordinates can be transformed into physical coordinates as follows:

$$\begin{pmatrix} \dfrac{\partial \alpha}{\partial x} \\ \dfrac{\partial \alpha}{\partial y} \end{pmatrix} = |\nabla_\xi \boldsymbol{x}|^{-1} \begin{pmatrix} \dfrac{\partial \alpha}{\partial \xi} \\ \dfrac{\partial \alpha}{\partial \eta} \end{pmatrix} \tag{3-2}$$

In the case of flows with free surfaces, the position of the mesh is not known a priori. The mesh must allow a relaxation of the physical domain. This makes the mapping part of the solution of the problem. The approach of a mobile mesh is detailed in the next section.

3.2.1
Formulation of Free Surface Problems

A set of the elliptical diffusion like equation has been successfully used in mapping free interface problems and was used in this work. Benjamin [31] proposed a generalization of the method developed by Christodoulou [32] and Christodoulou & Scriven [33], which bases on minimizing the functional that measures the smoothness, orthogonality and density of the mesh(Eq 3-3).

$$\int_\Omega (\boldsymbol{D}_\xi |\nabla\xi|^2 + \boldsymbol{D}_\eta |\nabla\eta|^2)d\Omega = 0 \tag{3-3}$$

The symbols $\boldsymbol{D}_\xi$ and $\boldsymbol{D}_\eta$ are the diffusion like coefficients of the coordinates potentials that control the spacing between the curves of constant ξ and η. The equations that minimize this functional are a pair of elliptic partial differential equations, similar to those found in heat transfer problems with variable thermal conductivity.

$$\nabla \cdot (\boldsymbol{D}_\eta \nabla\eta) = 0; \ \nabla \cdot (\boldsymbol{D}_\xi \nabla\xi) = 0 \tag{3-4}$$

Equations 3-4 are formulated in the physical domain. When the diffusion like coefficients are constant, equations 3-4 are reduced to the Laplace equation. The set of boundary conditions required to solve these pairs of partial differential equations is as follows.

Boundary Conditions for The Mapping

For both flows analyzed in this work, the following boundary conditions were applied.

1. **Fixed nodes**: used when the position of the nodes is known a priori.

2. **Nodal distribution prescribed**: used when the position of the nodes is known a priori and they respect functions of distribution.

$$\xi = f^{-1}(s), \ \eta = g^{-1}(s) \tag{3-5}$$

3. **Sliding over the boundary**: used when the nodes free to slide over a line which the equation is known.

$$f(\boldsymbol{x}) = 0 \tag{3-6}$$

5. **Kinematic condition**: used when there is no liquid flux across the interface. This condition couples the flow and the equations of the elliptic mesh generation method.

$$n \cdot u = 0 \tag{3-7}$$

3.3
Weighted Residual Form

The NS (eq.2-5) is discretized to set of equations 3-8 in the weak residue form, where each weighing-function ϕ_i generates one equation.

$$R_{m_i} = \int_\Omega \rho(\boldsymbol{u} \cdot \nabla \boldsymbol{u})\phi_i d\Omega + \int_\Omega \boldsymbol{T} : \nabla \phi_i d\Omega - \underbrace{\int_\Gamma (\boldsymbol{n} \cdot \boldsymbol{T})\phi_i d\Gamma}_{\boldsymbol{B.I.}} \tag{3-8}$$

The first two integrals refer to the interior of the domain computing the behavior of the fluid type defined in $\boldsymbol{T}$. The integral marked with B.I. (Boundary Integral) compute the derivative boundary conditions (Neumann boundary condition) as in the definitions of developed flows, lines of symmetry and free surfaces.

The following step details the construction of the boundary integral along the liquid-gas interfaces. Let $\boldsymbol{\omega}$ be the weight function.

$$B.I. = \int_\Gamma \left(\boldsymbol{n} \cdot \boldsymbol{T} \right) \cdot \boldsymbol{\omega}\, ds$$

$$B.I. = \int_\Gamma \left[\nabla_\Gamma \cdot \left(-p\boldsymbol{I} + \boldsymbol{\sigma}_\Gamma \right) \right] \cdot \boldsymbol{\omega}\, ds$$

$$B.I. = \int_\Gamma \nabla_\Gamma \cdot \left[\left(-p\boldsymbol{I} + \boldsymbol{\sigma}_\Gamma \right) \cdot \boldsymbol{\omega} \right] ds - \int_\Gamma \left(-p\boldsymbol{I} + \boldsymbol{\sigma}_\Gamma \right) : \nabla_\Gamma \boldsymbol{\omega}\, ds$$

$$B.I. = \left[\left(-p\boldsymbol{I} + \boldsymbol{\sigma}_\Gamma \right) \cdot \boldsymbol{\omega} \right]\Big|_{s_i}^{s_f} - \int_\Gamma \left(-p\boldsymbol{I} + \boldsymbol{\sigma}_\Gamma \right) : \nabla_\Gamma \boldsymbol{\omega}\, ds$$

The weak form of the mass and the diffusion like coefficients complete the set equations associated to the bulk.

$$R_{c_i} = \int_\Omega (\nabla \cdot \boldsymbol{u})\zeta_i d\Omega \tag{3-9}$$

$$R_{\xi_i} = \int_\Omega \nabla \cdot (D_\xi \nabla \boldsymbol{\xi})\phi_i d\Omega \tag{3-10}$$

$$R_{\eta_i} = \int_\Omega \nabla \cdot (D_\eta \nabla \boldsymbol{\eta})\phi_i d\Omega \tag{3-11}$$

Velocity and pressure fields expanded in terms of the basis functions

Each unknown field of the problem is expanded in a linear combination of a finite number of basis functions. For this work, the basis functions attend

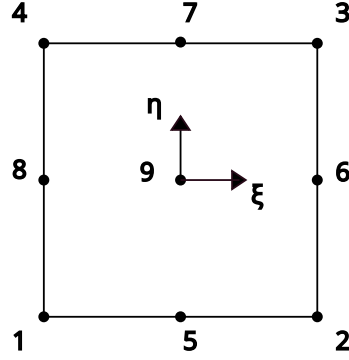the quadrangular elements with nine degrees of freedom as Figure 3.1.

Figure 3.1: Representation of the quadrangular element.

To obey the Babuska-Brezzi condition [34, 35], the basis functions were nine Lagrangian biquadratic functions, $\phi_{1,2..9}$, for the mesh and velocity, and three linear discontinues functions, $\zeta_{1,2,3}$, for the pressure. Therefore, the mesh, velocity and pressure variables assume:

$$\boldsymbol{x} = \begin{bmatrix} x \\ y \end{bmatrix} = \begin{bmatrix} \sum_{j=1}^{9}(X_j\phi_j); \\ \sum_{j=1}^{9}(Y_j\phi_j) \end{bmatrix}, \tag{3-12}$$

$$\boldsymbol{u} = \begin{bmatrix} u \\ v \end{bmatrix} = \begin{bmatrix} \sum_{j=1}^{9}(U_j\phi_j); \\ \sum_{j=1}^{9}(V_j\phi_j) \end{bmatrix}, \tag{3-13}$$

and

$$p = \sum_{j=1}^{3}(P_j\zeta_j). \tag{3-14}$$

The coefficients used in the linear P_j, U_j, V_j, X_j, and Y_j are unknown and part of the solution.

3.4
Solution Method

The integrals of the residual formulation are solved in the reference domain, Ω_0, using the Gaussian Quadrature Method with three points of integration in each direction. The weighted residual method together with a linear interpolation of the unknown fields give rise to a system of non-linear algebraic equations which is solved with Newton's method with a numerical

Jacobian. This system can be treated as $\boldsymbol{R}(\boldsymbol{c}) = 0$, where $\boldsymbol{c} = \boldsymbol{c}(\boldsymbol{u}, p, \boldsymbol{x})$ is the global solution vector and $\boldsymbol{R}$ is a global residual vector. Newton's method linearizes the system of non-linear algebraic equations and consists in the solution of this linear system by means of the following iterative procedure:

$\boldsymbol{c} = \boldsymbol{c_0}$
while $|\boldsymbol{R}(\boldsymbol{c})| > \epsilon$ **do**
    $\boldsymbol{J}\Delta\boldsymbol{c} = -\boldsymbol{R}$
    $\boldsymbol{c} = \boldsymbol{c} + \Delta\boldsymbol{c}$
end while

Here, ϵ is the numerical tolerance of the method, $\boldsymbol{c_0}$ is an initial guess and $\boldsymbol{J}$ is the Jacobian matrix that denotes the sensibility of each residual equation in relation to each unknown vector variable of the problem $\boldsymbol{c}$.

$$J_{ij} = \frac{\partial R_i}{\partial c_j} \tag{3-15}$$

3.5
Mesh Construction

3.5.1
Extrusion

An advantages of using dimensionless parameters is to bring together several simulations in a few. Both the capillarity and Boussinesq numbers take the dimensions of the flow into account (indirectly in the case of capillarity). Thus, the length of the section within the die only needs to ensure that the inflow boundary is far enough to not affect the flow near the exit of the channel and the outflow plane is far enough for the flow to become fully developed.

The differences between these two regions make natural split the mesh in two parts, which one with its own length, numbers of elements and boundary conditions. Figure 3.2 shows the division of the mesh to fit the physical domain (Figure 2.1). Region 1 is associated with the interior of the die and region 2 is associated with the free surface flow. The length of the die is eight time the channel height ($8H$) and the free flow length is ten times the channel height ($10H$). These two measures must be checked according to the hypotheses. The values n1, n2 and n3 symbolize the number of elements in each division. They are, respectively, the number of horizontal elements in region 1 (n1), region 2 (n2) and the number of vertical elements of both regions (n3).
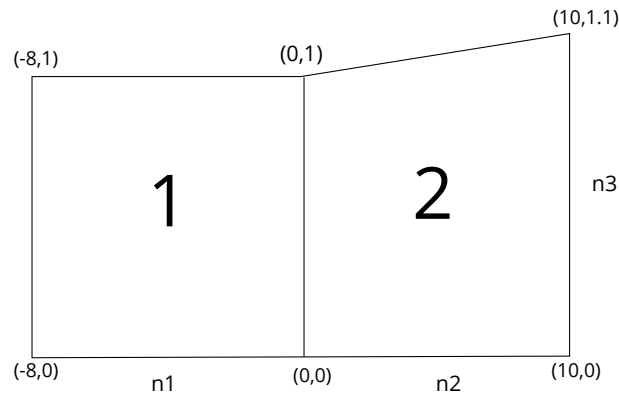
Figure 3.2: The division of the mesh adjusted the physical domain. In parentheses are the coordinates of the vertices of the mesh. The values n1, n2 and n3 symbolize the amount of elements in each division.

For our extrusion flow analysis, the capillary number will not exceed 2 and the Boussinesq will not exceed 15. Then, the mesh using these two values covers the whole set of values investigated in the results and discussions section. Four meshes were constructed to evaluate the solution and check the mesh independence. The first analysis discuss about the length to achieve the fully developed flow state. Four meshes with different free flow lengths were tested: 10H, 16H, 20H and 24H. The number of elements n2 is proportional to this values. The table 3.1 summarizes the details of mesh construction.

Table 3.1: Test meshes characteristics for the extrusion flow.

Properties	mesh 1	mesh 2	mesh 3	mesh 4
Capillary (Ca)	2	2	2	2
Boussinesq (Bq)	15	15	15	15
Free Flow Lengths	10H	16H	20H	24H
n1	25	25	25	25
n2	35	42	70	84
n3	15	15	15	15

Figure 3.3 shows mesh 1 and is representative of the four meshes because they only differ in the number of element.
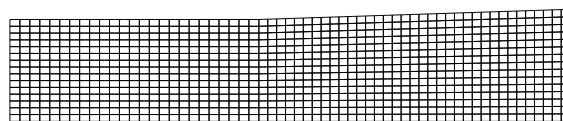

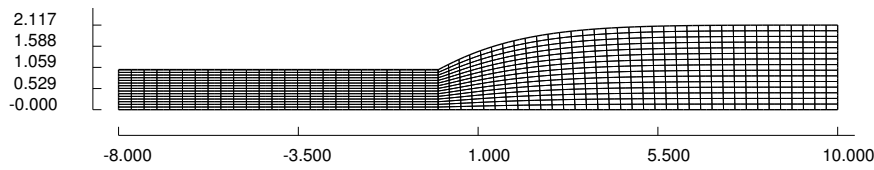Figure 3.3: Mesh 1: region 1 with 25X15 and region 2 with 35X15.

Figure 3.4: The final position of the mesh 3. The rearrangement of this mesh is representative of the three meshes due the very similar performance.

Again, Figure 3.4 shows the flow configuration obtained with mesh 3 because it is representative of the three meshes that had a very similar performance. Figure 3.4 also demonstrates the operation of the mesh. The mobile mesh allowed the line defining the boundary of the fluid in region 2 to form an arched profile while the elements just below this line have been redistributed so as to homogeneous division of the elements. As expected, the guessed value for the expansion of the mesh was altered by the numerical iterations.

Table 3.2: Test meshes characteristics for the extrusion flow (more refined).

Properties	mesh 1	mesh 2	mesh 3	mesh 4
Length	10	16	20	24
Final Thickness	2.9648	3.0742	3.0899	3.0854

Table 3.2 presents the final position of the surface for each mesh. The final position of the surface varied slightly for each domain. Since the number of vertical elements was not tested, a second set of meshes was made to evaluate if the final position oscillation can be attenuated by increasing n3. For this test, only the n3 was altered form 15 to 20 in all meshes, as shown in table 3.3.

Table 3.3: Test meshes characteristics for the extrusion flow (more refined).

Properties	mesh 1	mesh 2	mesh 3	mesh 4
Capillary (Ca)	2	2	2	2
Boussinesq (Bq)	15	15	15	2
Free Flow Lengths	10H	16H	20H	24H
n1	25	25	25	25
n2	35	42	70	84
n3	20	20	20	20

Table 3.4 shows that the meshes have a better agreement. For this test, the meshes 2, 3 and 4 had a minor variation in the final thickness. So, mesh 2 is enough to analyze the interfacial viscosity in the next session.

Table 3.4: Test meshes characteristics for the extrusion flow (more refined).

Properties	mesh 1	mesh 2	mesh 3	mesh 4
Length	10	16	20	24
Final Thickness	3.0510	3.0812	3.0849	3.0832

3.5.2
Slot Die Coating

Because we are mostly interested on the dynamics of the film formation region and on the low flow limit, we restrict our analysis on the downstream meniscus of a slot coating process, as done by Romero *et al* [6]. The flow domain is divided in three regions, as shown in Figure 3.5. The variables n1, n2, n3 and n4 represent the number of elements on each boundary side. The number of horizontal elements of region 1 and region 2 are respectively n1 and n2 and the vertical elements of region 1 and region 2 are respectively n3 and n4. The region 3 that is connected with regions 1 and 2 has n4 elements at horizontal and n3 elements at vertical.
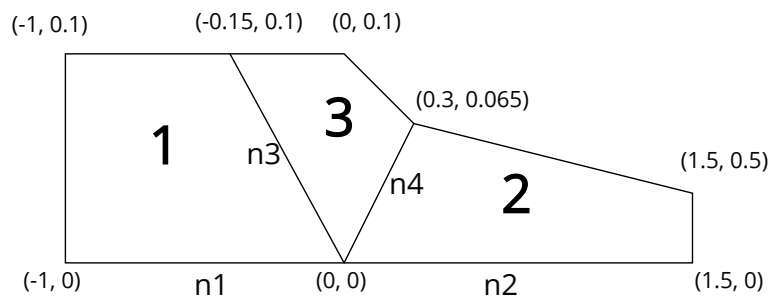

Figure 3.5: Slot Die regions distribution.

The distribution of elements in the mesh is n1 = 25, n2 = 80, n3 = 15 and n4 = 15. The mesh with equally spaced elements is shown in Figure 3.6.
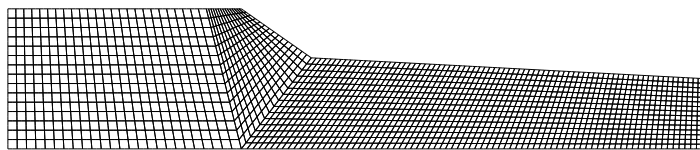

Figure 3.6: Slot Die elements distribution.

In our tests, the capillary number will not exceed 2 and the Boussinesq will not exceed 15. Then, the mesh using these two values covers the whole set of values investigated in the results and discussions section. Different from the extrusion problem, the coating velocity and the position of the interface at the end of the domain are known a priori. The mesh 1 is defined at tab 3.5 and answer the boundary conditions at the end of the domain.

Table 3.5: Test meshes characteristics for the slot die coating flow

Properties	mesh 1
Capillary (Ca)	2
Boussinesq (Bq)	15
Dimensionless Flow Rate	0.5
Coated Layer Thickness	0.5H
Free Flow Length	20H
n1	25
n2	80
n3	20
n4	20

The figure 3.7 shows the mesh 1 after the simulation.
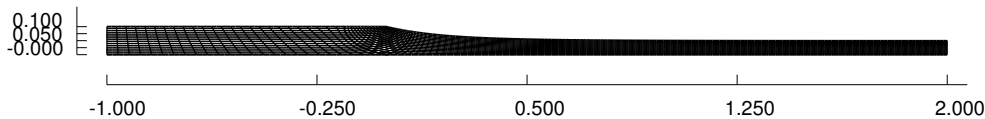

Figure 3.7: Mesh 1: region 1 with 25X20, region 2 with 80X20 and region 3 with 20X20.

Figure 3.8 shows that the surface velocity reaches the substrate velocity at the end of the domain, which means that the outflow profile is uniform.

Figure 3.9 shows that the interface reaches the defined height as 0.05. For this operating conditions, the length of twenty times the gap to the liquid layer was sufficient to guarantee the development of the flow. But for higher values to the Boussinesq number or lower to the capillarity number, this length should be increased to enhance the reliability of the simulation.
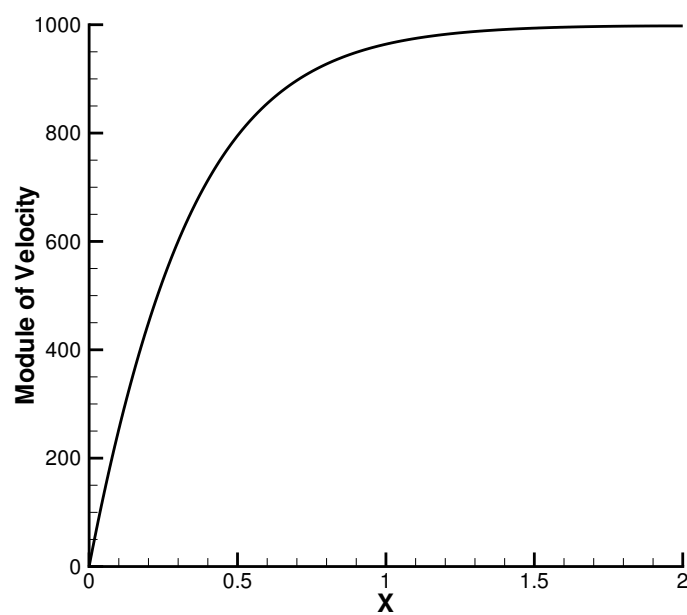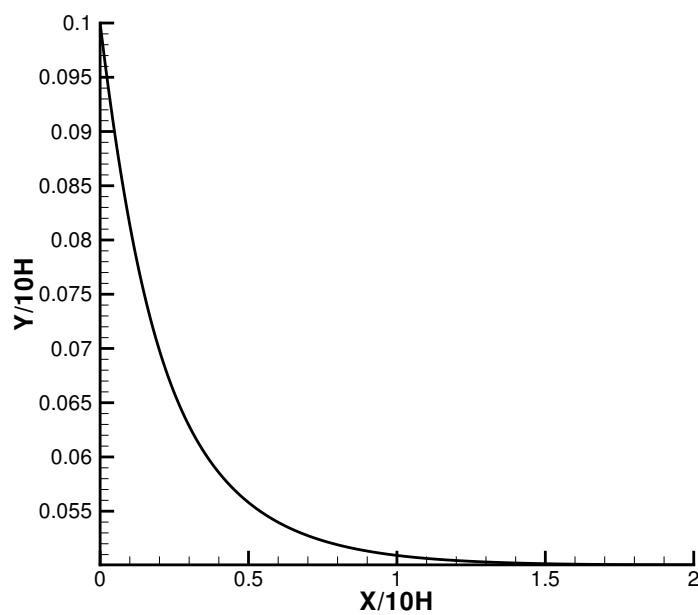
Figure 3.8: Velocity profile of mesh 1.

Figure 3.9: Interface profile of mesh 1.

After the constructions of the meshes for extrusion and coating flows, the chapter of results and discussions deals with how the dimensionless numbers affect each flow.

4
Results and Discussions

This chapter presents the results for both the extrusion and slot coating flow. The focus is to study the effect of the interface viscosity, represented by the Boussinesq number (Bq) on the flow pattern.

4.1
Extrusion Flow

For Newtonian fluid, the flow inside the die has a parabolic velocity profile, after it goes out the exit, it gradually becomes a plug flow. The extrudate swelling can be observed in the mesh test of the previous section. The increasing of the thickness is not expected to exceed 10% for Newtonian case [3].

Characterized by a over dilatation of the extrusion dimensions, the Die-Swell is a phenomenon that occurs in extrusion of polymers. The extra swell is associated with the rheological behavior of the liquid. Here we focus on die-swell flow of Newtonian liquids (bulk) with complex interface.

High capillary numbers can be generated by high speed or a very low surface tension. In both cases, the flow is dominated by viscous forces. Higher viscosity leads to stronger internal stress and consequently a greater swelling effect. Even for a high speed, the scale of the problem makes the Reynolds number lower than unit and guarantees the hypotheses of stokes problem. As the mathematical formulation was done considering the fully Navier Stokes problem, the Stokes was recovered considering the specific mass of the fluids equals zero in the NS equation.

For $Bq \ll 1$, the flow is dominated by the bulk stress and for $Bq \gg 1$ the surface stress becomes relevant to the flow behavior. So three values were selected to be examined corresponding to a flow dominated by the bulk viscosity (Bq = 0), another dominated by interface viscosity (Bq = 10) and a last one in which both forces have the same order of magnitude (Bq = 1).

To investigate what happens when the fluid is Newtonian but with a complex interface different values of the surface viscosity were defined while the others parameters were kept constant.

4.1.1
Low Capillarity Number

At low capillary number, the flow is dominated by surface tension forces. The viscous normal force that is responsible for the extrudate swell is weak compared to the surface tension. As a consequence, the free surface is almost flat and intensity of extrudate swell is very small. We analyzed the effect of Bq at Ca equal to 10^{-3}, as indicated in Table 4.1.

Table 4.1: Dimensionless group for the low capillary extrusion flow.

Properties	Case 1	Case 2	Case 3
Capillary (Ca)	10^{-3}	10^{-3}	10^{-3}
Boussinesq (Bq)	0	1	10

The results obtained for the flow field are present in Figures 4.1, 4.2 and 4.3. The color contours represent the dimensionless pressure field. The color code is the same for the three graphs and shows that the inlet pressure increases as the interface viscosity increases. Near the exit of the die, the inclination of the streamlines is higher in the non-viscous surface. When the interface is viscous, the liquid acceleration along the interface is slower, as show in Figure 4.4. The terminal velocity is also smaller for high Bq, which leads to a stronger die swell, as show in Figure 4.5. It is important to note that at the low Ca, the extrudate swell is small for all cases.
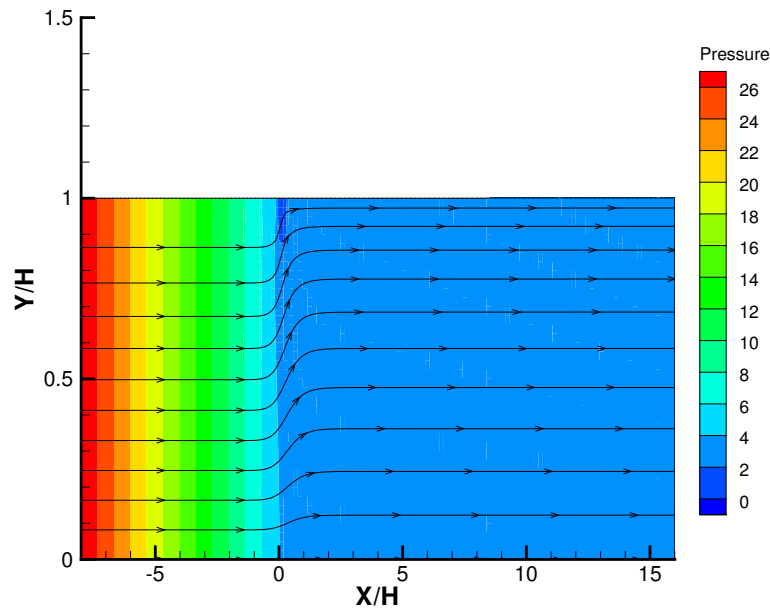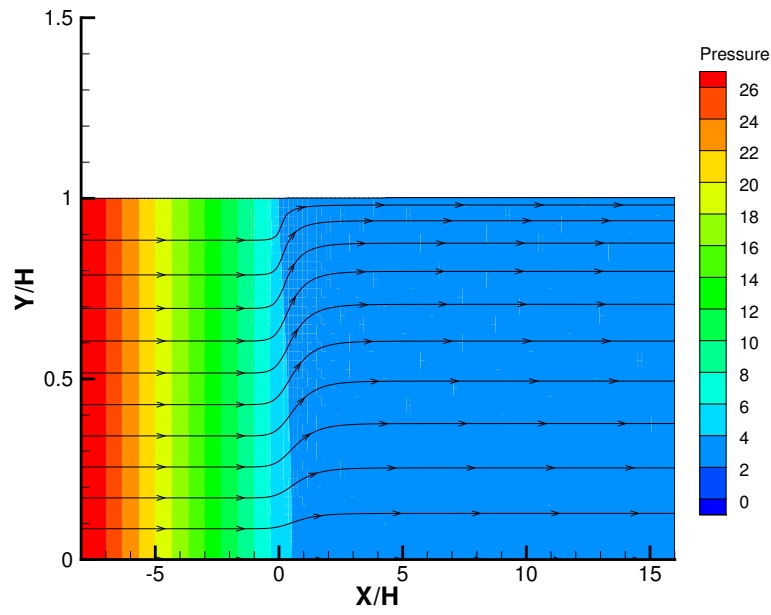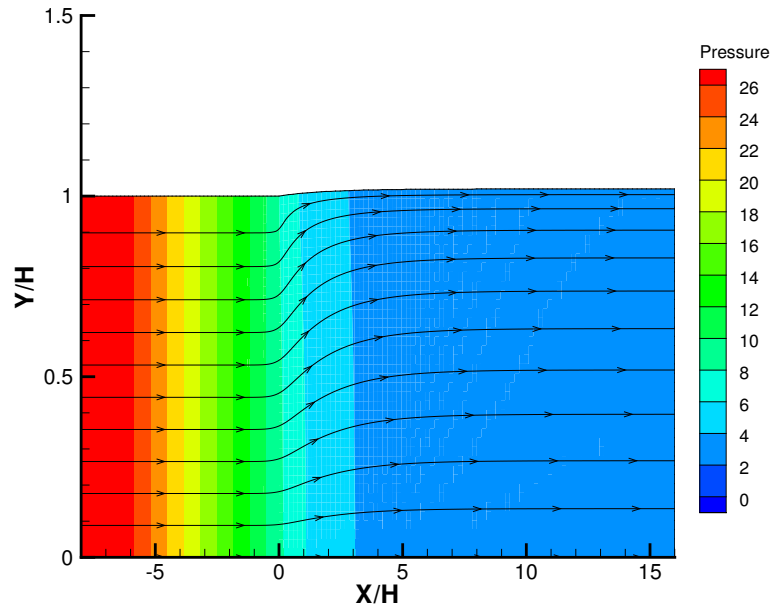
Figure 4.1: Pressure field and Streamlines for Bq $= 0$ and Ca $= 10^{-3}$

Figure 4.2: Pressure field and Streamlines for Bq = 1 and Ca = 10^{-3}

Figure 4.3: Pressure field and Streamlines for Bq = 10 and Ca = 10^{-3}
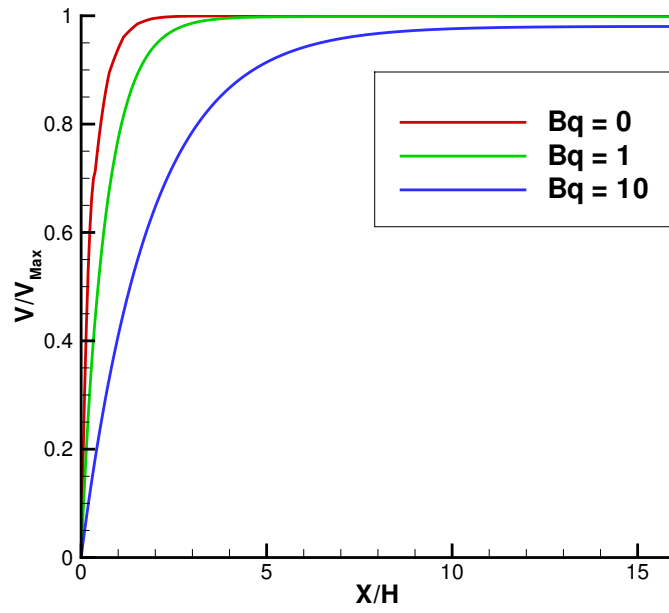
Figure 4.4: Velocity profile along the interface of the extrusion flow for different Boussinesq numbers and Capillarity number equal $1 \cdot 10^{-3}$.
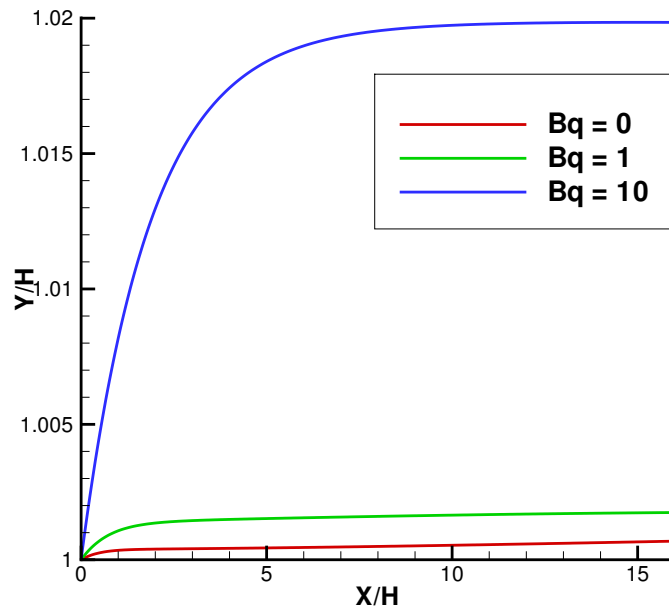

Figure 4.5: Surface profile extrusion flow for different Boussinesq numbers and Capillarity number equal $1 \cdot 10^{-3}$.

The surface viscosity generates friction that slows down the flow near the surface and propagates into the flow. This connects the surface shape with

the velocity profiles. The velocity in the beginning of the free surface is zero because of the no-slip condition at the wall of the channel and asymptotically grows to the terminal mean velocity at outlet. As the average velocity decreases affected by surface friction, the film thickness increases to preserves to the mass. In addition, since flow is retarded, development occurs farther from the outlet of the channel. Hence the smoothing of the speed curves is also related to the friction of the surface.
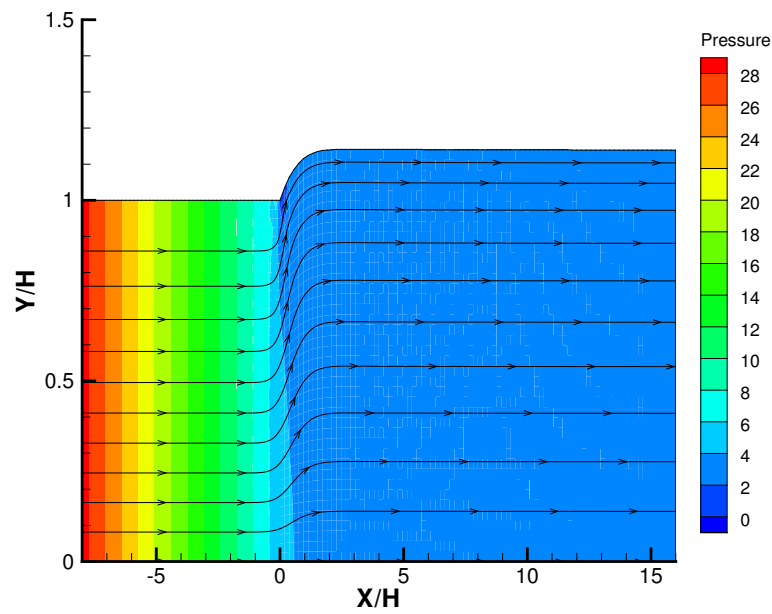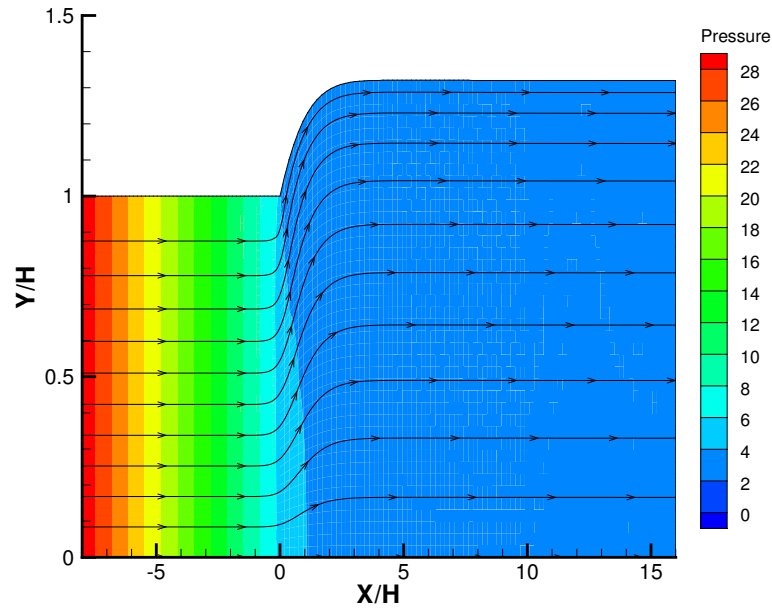
4.1.2
High Capillary Number

The behavior of the surface is quite different when the capillarity is increased. The influence of viscous forces further expand the film thickness and provides larger curvatures. This test uses the capillary number equal 1, which is 1000 times the value of the previous test, and a large swelling is expected. Table 4.2 resume the simulations.

Table 4.2: Dimensionless group for the high capillary extrusion flow.

Properties	Case 1	Case 2	Case 3
Capillary (Ca)	1	1	1
Boussinesq (Bq)	0	1	10

Figures 4.6, 4.7 and 4.8 show that the difference between the swelling is notorious and very pronounced for the higher Boussinesq number. The film thickness of a Newtonian fluid with a viscous interface increased over the expected value of Newtonian fluids with simple interface. This behavior was similar to extrusion of non Newtonian fluids. The pressure field also shows that the inlet pressure increases as the interface viscosity increases. Near the exit of the die, the inclination of the streamlines is much higher in the non-viscous surface than in the previous simulation because they follow the deformation of the surface.

Figure 4.6: Pressure field and Streamlines for Bq = 0 and Ca = 1

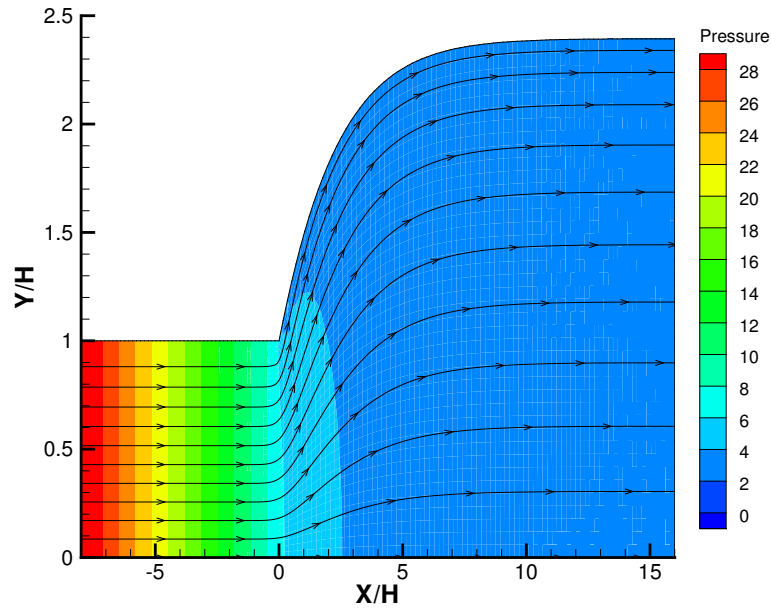Figure 4.7: Pressure field and Streamlines for Bq = 1 and Ca = 1

Figure 4.8: Pressure field and Streamlines for Bq = 10 and Ca = 1

The dimensionless pressure scale is the same for all three graphs. Figure 4.6 shows that the top of the channel output (x = 0) is a low pressure region. Comparing with Figure 4.7, when the moderate surface viscosity was included, A low pressure region takes place of the higher pressure region. It means that pressure has increased and that the pressure gradient has decreased. The same region in Figure 4.8 is occupied by low pressure values.

Figure 4.9 shows the surface profile for these three cases. The profile for the higher viscosity stands out against the other two. The velocity distribution along the free surface, in Figure 4.10, clearly show that viscous interfaces slows down the acceleration of the liquid along the free surface.
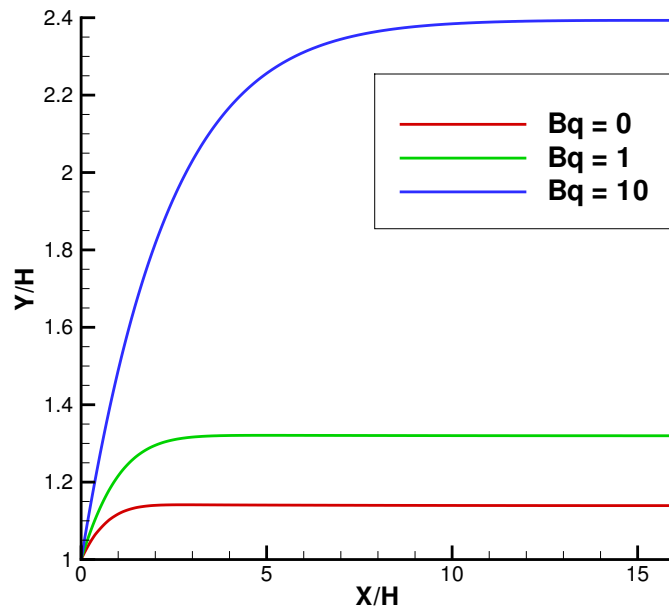
Figure 4.9: Surface profile of the extrusion flow for different Boussinesq numbers and Capillarity number equal 1.
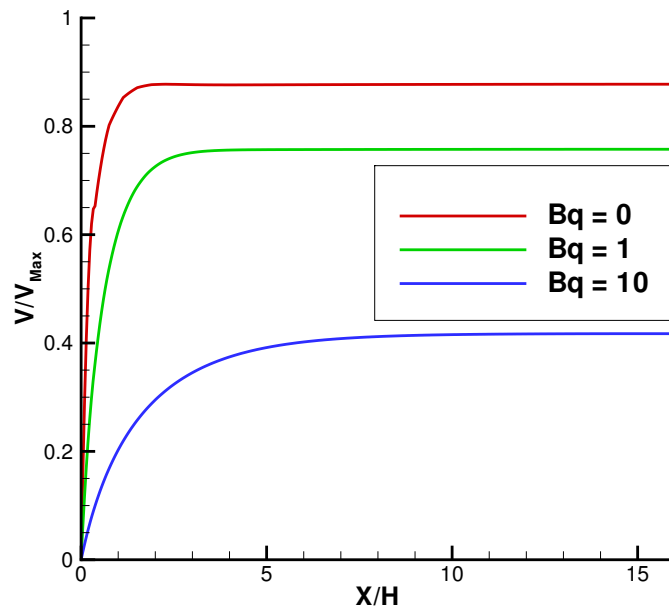

Figure 4.10: Velocity Surface profile of the extrusion flow for different Boussinesq numbers and Capillarity number equal 1.

Analyzing the previous results, it is already possible to observe that, in general, the interfacial viscosity softens the velocity and pressure gradient
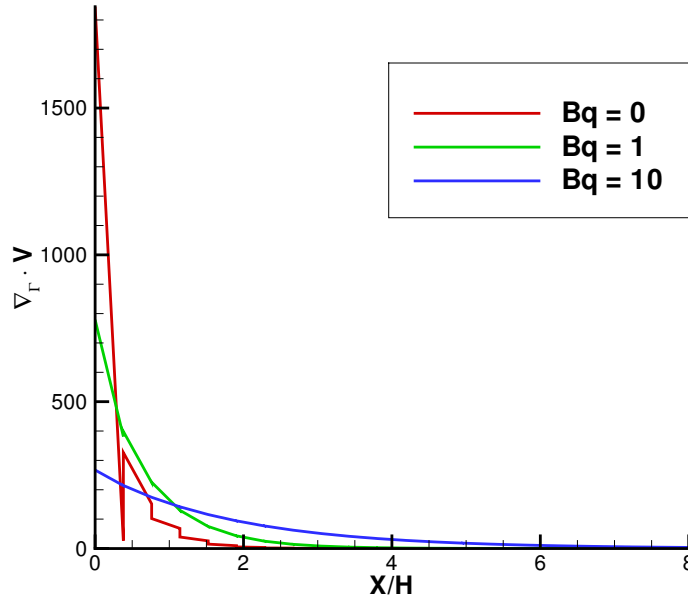
Figure 4.11: The profile of the interface divergent of velocity for the extrusion flow for Capillary number equal 10^{-3} and different Boussinesq numbers.

functions. This can lead to a significant increase in the extruded layer and a decrease in the speed of production. Figures 4.11 and 4.12 set the graph of the divergent of velocity along th interface for the capillarity 10^{-3} and 1.

Figure 4.11 shows that, for the three values of Boussinesq number, the interface divergent of velocity is a decreasing function that assumes zero at the end of the domain. The interface divergent of velocity depends on the projection of the velocity gradient along the surface. As the velocity gradient decreases, the divergent also has to decreases along the domain. The graph also shows that resistance to stretching appears when the surface viscosity is considered, holding the initial acceleration of the interface and at delaying the plug flow.

The oscillation of the free surface for the non-viscous interface occurs because the interface divergent is too intense. The absence of coupling between the divergent and the system of equations allows a greater variance of the speed and makes the mesh poor to compute this magnitude. The oscillations could be solved with a more refined mesh, but this was not the focus of this work.

As expected, Figure 4.12 shows that the surface bends more when the capillary increases, although the interface divergences of velocity along the interfaces are more intense in the simulations with the low number of capillarity. This function measures the difference of the displacement in the direction of the flow and responds to the stretching or shrinking. That is
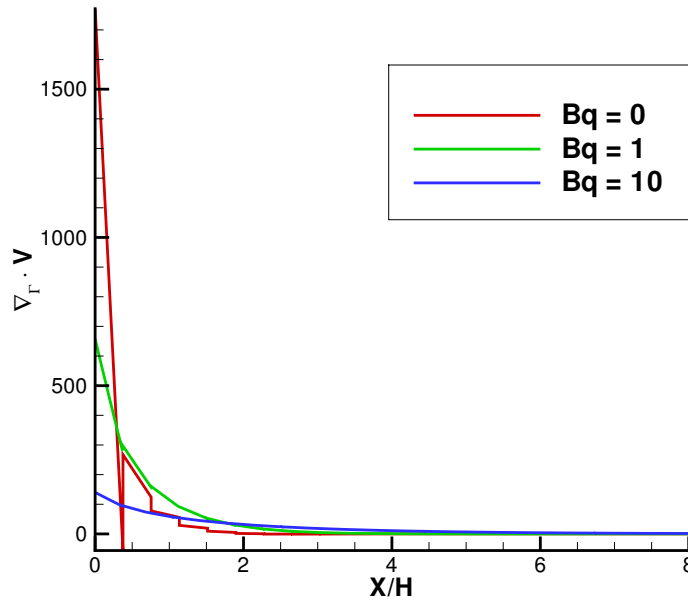
Figure 4.12: The profile of the interface divergent of velocity for the extrusion flow for Capillary number equal 1 and different Boussinesq numbers.

different to measure whether the surface is bending. So according to the results, the interface stretches less for a more significant capillarity numbers, and the stretching occurs closer to the die. Therefore, the low capillarity may prevent the bending of the surface, but pushes forward the development of the flow.

Figure 4.13 shows a plot that summarizes the behavior of the viscous surfaces. The complex behaviour creates a resistance to stretching and reduces the speed of the flow, and as a consequence due to mass conservation increases the film thickness. In the case of low numbers of capillarity, surface tensions limits the deformation of the surface. Then the effect of viscosity is more evident for high capillarity. The scale is a semi-log. Then the graph also shows that the influence of the surface viscosity can be more significant to the terminal thickness than the capillarity. For much higher numbers of Boussinesq, the interface expands over the domain.
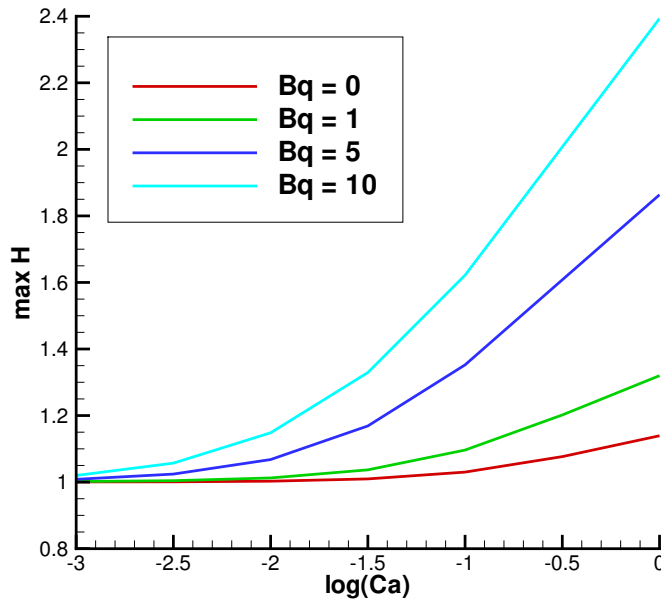
Figure 4.13: Maximum film thickness vs capillary number for various Boussinesq number values.

4.2
Downstream region of Slot Coating Flow

The slot die coating is a pre-metered coating method, because the film thickness is setted by the flow rate and web speed area, and it is independent of the other process condition. This section studies how the interfacial viscosity changes the flow pattern in the film formation region.
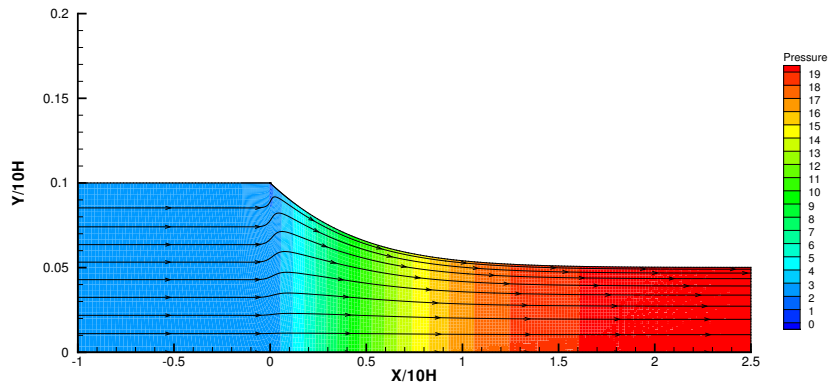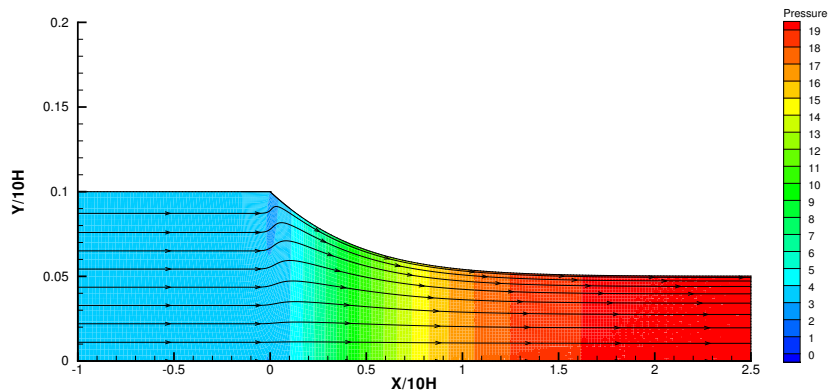
4.2.1
Low Capillarity Number

Low capillary number flows are dominated by surface tension forces. High surface tensions leads to small interface curvature. Then, the interface should have a smooth transition between the contact line with the die and the terminal height of the film. The dimensionless flow rate was set as 0.5. Then, the film thickness is the half of the gap. The first simulation analyzes this fact maintaining the capillary number equal to 10^{-3} and varies the Boussinesq number between 0, 1 and 10, as shown in table 4.3.

Table 4.3: Dimensionless group for the low capillary slot die coating flow.

Properties	Case 1	Case 2	Case 3
Capillary (Ca)	10^{-3}	10^{-3}	10^{-3}
Boussinesq (Bq)	0	1	10
Dimensionless Flow Rate	0.5	0.5	0.5

The flow field results are presented in Figures 4.20, 4.21 and 4.22. The color contours represent the dimensionless pressure field. The color code is the same for the three graphs and shows that the inlet pressure increases as the interface viscosity increases. Then, the pressure gradient decreases as the Boussinesq number is increased. Near the exit of the die, the inclination of the streamlines is also higher in the non-viscous surface. When the interface is viscous, the liquid acceleration along the interface is slower, as show in Figure 4.18 and the curvature is also smaller for high Boussinesq numbes, as show in Figure 4.17.

Figure 4.14: Pressure field and Streamlines for Bq = 0 and Ca = 10^{-3}

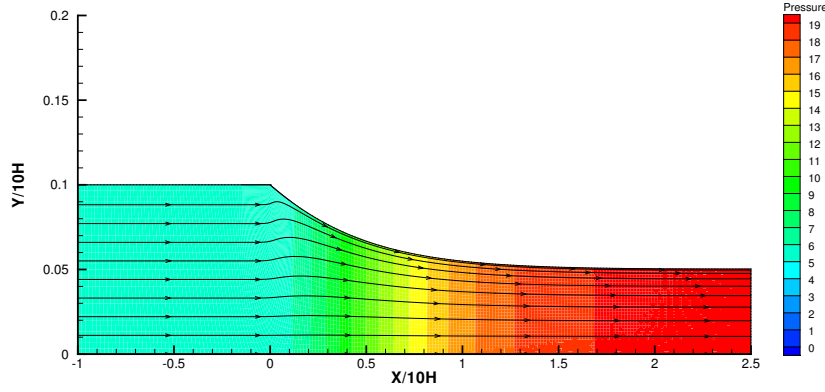Figure 4.15: Pressure field and Streamlines for Bq = 1 and Ca = 10^{-3}

Figure 4.16: Pressure field and Streamlines for Bq = 10 and Ca = 10^{-3}

The gap between the slot die and the substrate was fixed and for all cases the interface profile start at the same point. As the flow rate and the substrate velocity are the same for the test, all the curves end at the same point. The difference among the curves is due to the curvature of the meniscus. Figure 4.17 shows the interfacial position for the three values of surface viscosity. As the fluid takes longer to speed up, the film takes longer to reach the terminal thickness.

Figure 4.18 shows the graph of velocity on the free surface. All the curves start from zero because of the no-slip condition at the wall and grows until the substrate velocity reaches an asymptotic value. The difference between the speed and interface profiles shows that the surface viscosity delayed the development of the flow.

The divergent of velocity on the surface is a key concept to understand this phenomenon. It defines the location and the intensity of the tension. The graph on Figure 4.19 shows that the interface deformation is greater near the channel output where the fluid accelerates from zero to the substrate velocity. The extra tension generated by the divergent holds the deformation what makes the initial value of the curve be smaller for the cases with interfacial viscosity. On the other hand, the deformation occurs for a larger length. Near the end, the divergent tends to zero. So the difference among the three cases tends to disappear far from the slot die. Higher the number of Boussinesq, greater the resistance of the surface to the deformation. At the plug flow when the surface is not deforming, there is no extra surface tension, even for high values of Boussinesq.
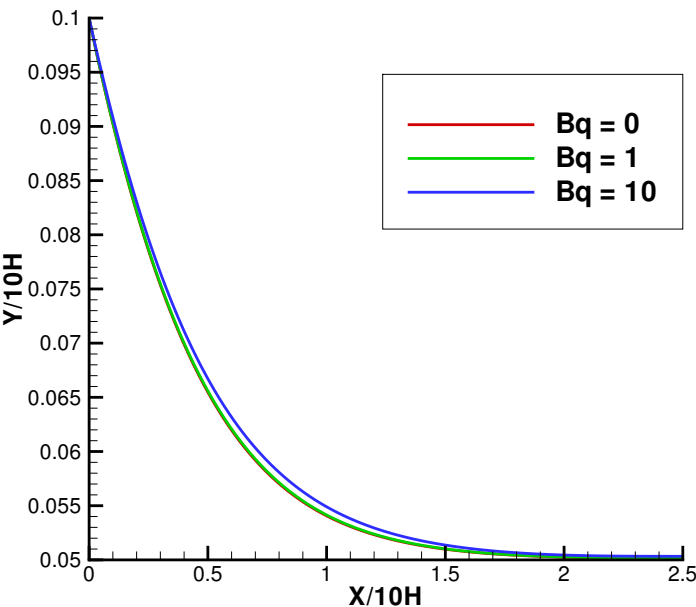
Figure 4.17: Surface profile of the slot die coating flow for different Boussinesq numbers and Capillarity number equal 10^{-3}.
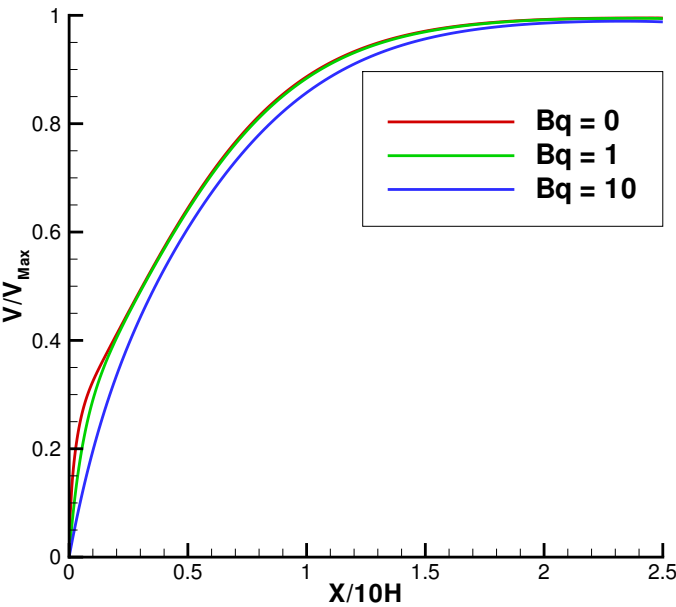

Figure 4.18: Velocity profile of the slot die coating flow for different Boussinesq numbers and Capillarity number equal 10^{-3}.
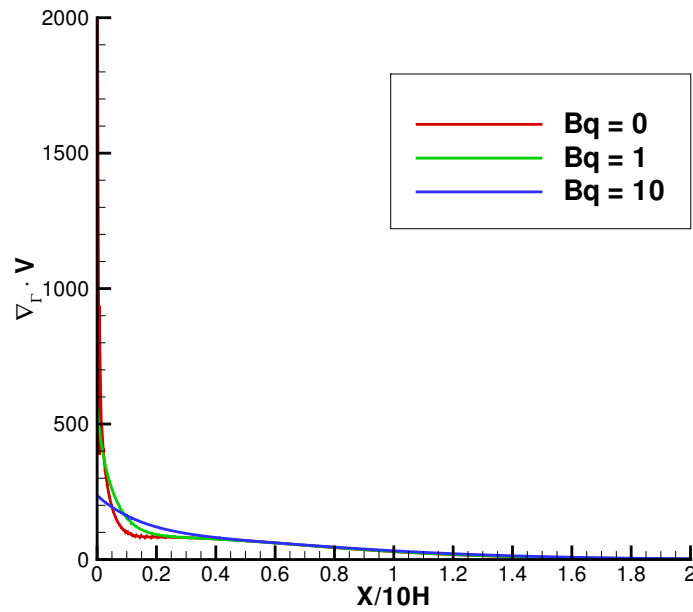
Figure 4.19: The profile of the interface divergent of velocity for the slot coating flow for Capillary number equal 10^{-3} and different Boussinesq numbers.

4.2.2
High Capillary Number

For high capillary number, the flow is dominated by viscous forces leading to increase of the curvatures. This simulation reduced the surface tension such that the capillary number is equal to 1. The Boussinesq number varies between 0, 1 and 10, as shown in the Table 4.4.

Table 4.4: Dimensionless group for the low capillary slot die coating flow.

Properties	Case 1	Case 2	Case 3
Capillary (Ca)	1	1	1
Boussinesq (Bq)	0	1	10
Dimensionless Flow Rate	0.5	0.5	0.5

Figures 4.20, 4.21 and 4.22 display the results of this simulation. The increase of the capillary number anticipated the development of the coating flow and accentuated the differences in curvatures due to surface viscosity. The pressure values also have changed, but the pressure gradient still decreases as the Boussinesq number is increased.
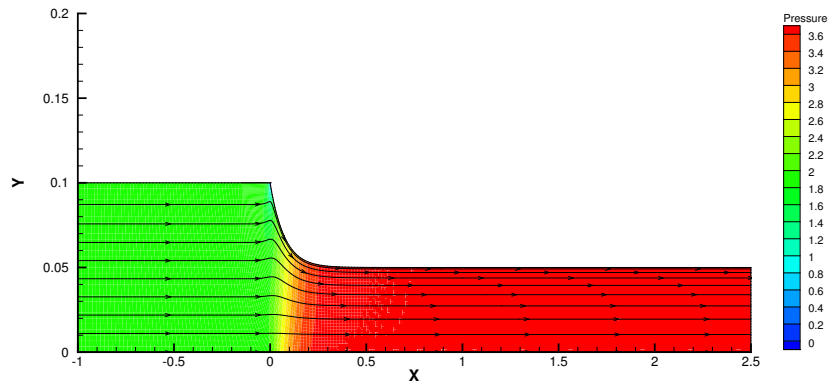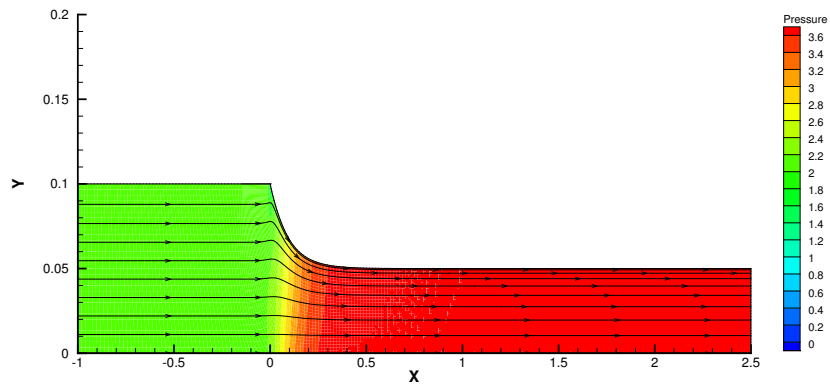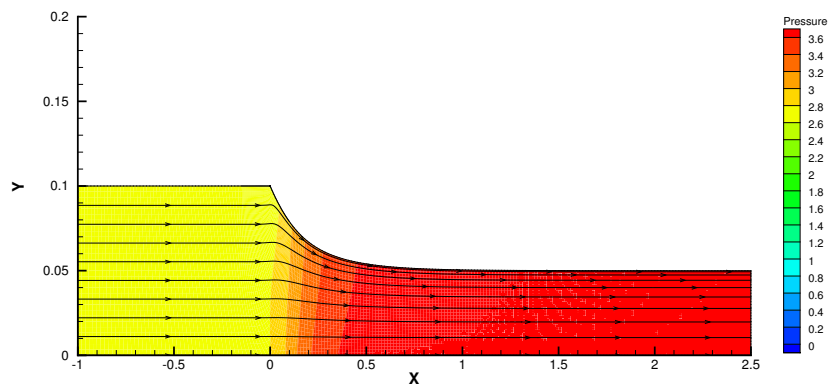
Figure 4.20: Pressure profile and Streamlines for Bq = 0 and Ca = 1

Figure 4.21: Pressure profile and Streamlines for Bq = 1 and Ca = 1

Figure 4.22: Pressure profile and Streamlines for Bq = 10 and Ca = 1

Figure 4.23 shows the interfacial position and Figure 4.24 the velocity along the downstream meniscus for the three values of surface viscosity.

Although the position of the interface has changed, the interfacial viscosity have reduced the flow acceleration and delayed flow development.
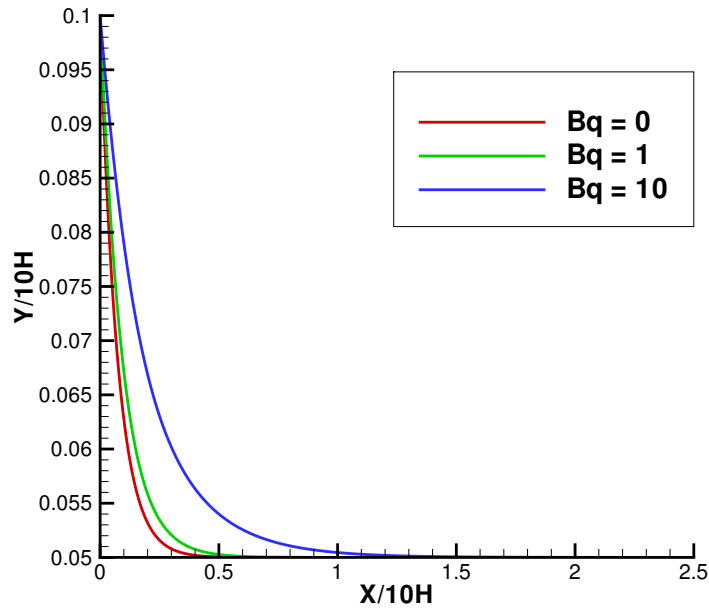

Figure 4.23: Surface profile of the slot die coating flow for different Boussinesq numbers and Capillarity number equal 1.
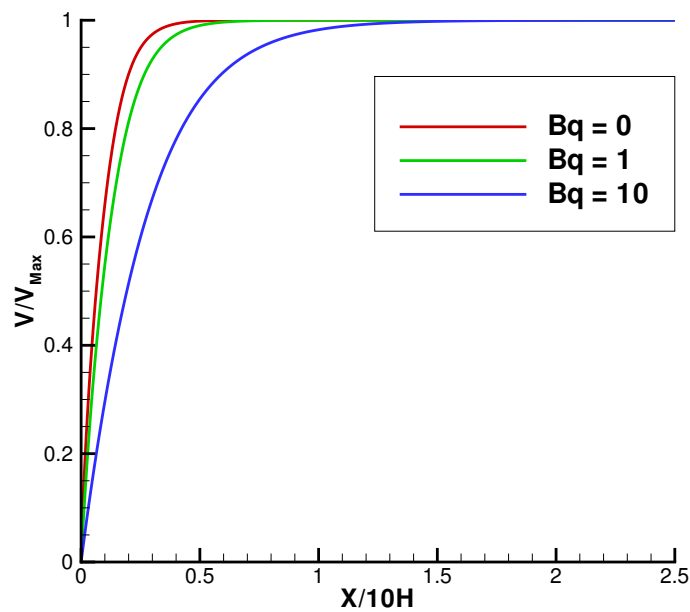

Figure 4.24: Velocity profile of the slot die coating flow for different Boussinesq numbers and Capillarity number equal 1.

The surface bends more when the capillary increases. So according to the graph in Figure 4.25, interface stretches more for significant capillarity numbers. Increasing the Boussinesq number pushes forward the development of the flow.
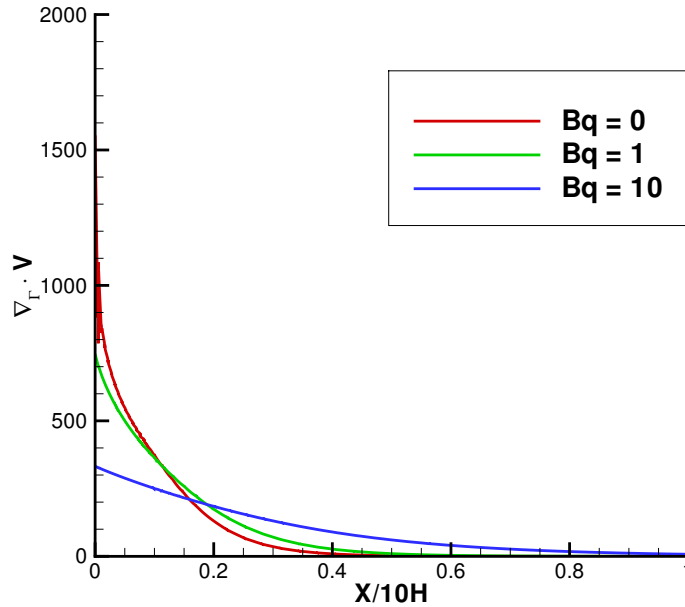

Figure 4.25: The profile of the interface divergent of velocity for the slot coating flow for Capillary number equal 1 and different Boussinesq numbers.

Up to now, the behavior of the coating process has been similar to that of the extrusion of fluid. This shows that the mechanism of action of interfacial viscosity is the same that the extrusion. The divergent on the surface does not measure whether the surface is bending or flatting, but if it is stretching or shrinking. The graphs of the divergent on the surface for the capillarity 10^{-3} and 1 show the deformations are still occurring near to die.

For both capillarity numbers considered here, the fluid extrusion and coating simulations maintained the constant flow rate and varied the surface tension. This partly explains the similarity in the results, since for the extrusion process, the film terminal thickness is not determined only by the capillarity, as in the case of coating. The next subsection will deal with the coating behavior when the flow rate is reduced to very small values.

4.2.3
Low-flow limit

Increasing the speed of the substrate while maintaining a constant flow rate, decreases the terminal height of the film and allows productions of

thinner films. The excessive film thickness reduction may initiate a failure mechanism called Low-flow limit [6]. A insufficient volume of fluid feeding the apparatus generates entrance of fluid in the cavity leading to irregularities and compromising the coating uniformity.

This low-flow limit is preceded by an intensification in the curvature of the meniscus downstream. Figure 4.26 shows a schematic representation of the downstream meniscus bending that may lead to coating bead breakup. The downstream contact angle θ is a measure of the meniscus retreat. This section analyzes how the interfacial viscosity affects the entrance of fluid in the cavity, by monitoring the contact angle and varying the flow rate while fixing the capillary number.
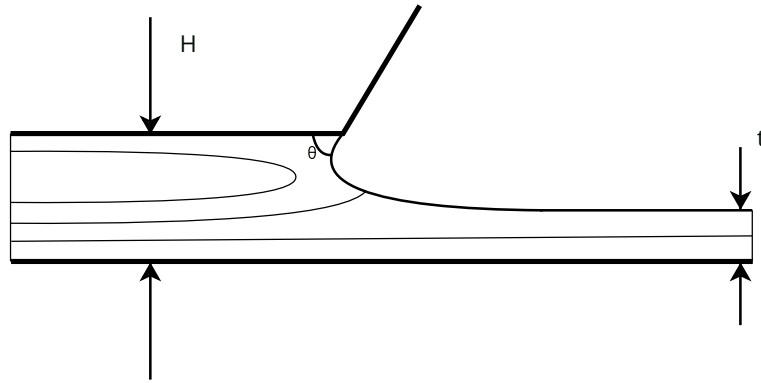

Figure 4.26: Low Flow Limit Scheme

A set of simulations was done to evaluate the response of the angle as a function of flow rate for different values of Boussinesq numbers. The mesh of theses simulations was the same as the previous section and the capillary number was equal to 0.2. The Boussinesq number varies between 0, 1, 5 and 10, as shown in table 4.5.

Table 4.5: Dimensionless group for the low capillary slot die coating flow.

Properties	Fluid 1	Fluid 2	Fluid 3	Fluid 4
Capillary (Ca)	0.2	0.2	0.2	0.2
Boussinesq (Bq)	0	1	5	10

The results of the simulations are shown in Figure 4.27 where the vertical axis shows the downstream static contact angle and the horizontal axis shows the ratio between the gap size and the film thickness $\frac{H}{t}$. As the gap H is constant, thinner film thickness leads to right positions in abscissa.

All curves have an asymptotic value, which indicates that there is a minimum thickness above which it is possible to coat a substrate. The graph
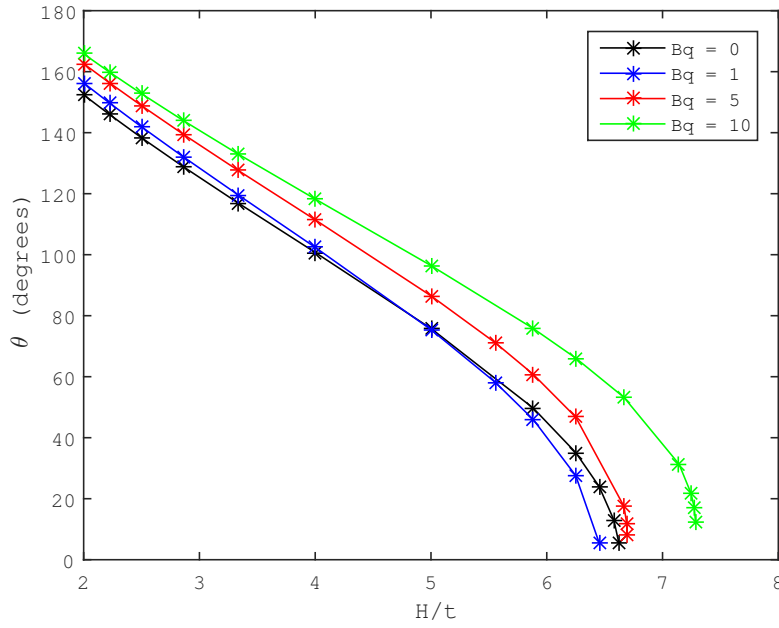
Figure 4.27: A set of simulations that evaluate response of the angle of reentrance and the thickness to the flow rate and the Boussinesq number.

also shows that it is possible to reduce the minimum thickness by increasing the surface viscosities.

The result in Figure 4.28 shows that this thickness also depends on the interfacial viscosities since different values of minimum width can occur for the same flow rate.

An important fact arising from the non-linearity of the flow is that a small viscosity has the effect of increasing that minimum thickness. This shows that even a tiny interfacial viscosity may not be negligible.

Figure 4.29 shows the velocity field in the region between the meniscus and the downstream lip for Ca equals to 0.1 and the dimensionless flow rate equals 0.16. The Boussinesq number varies between 0, 1, 5 and 10, as shown in the table 4.6.

Table 4.6: Dimensionless group for the low capillary slot die coating flow.

Properties	Case 1	Case 2	Case 3	Case 4
Capillary (Ca)	0.2	0.2	0.2	0.2
Boussinesq (Bq)	0	1	5	10
Dimensionless Flow Rate	0.16	0.16	0.16	0.16

The coating at this dimensionless flow rate induces a recirculation under the downstream lip. The viscous force resisting to the deformation along the free surface alter the velocity of fluid near the surface. As the interface
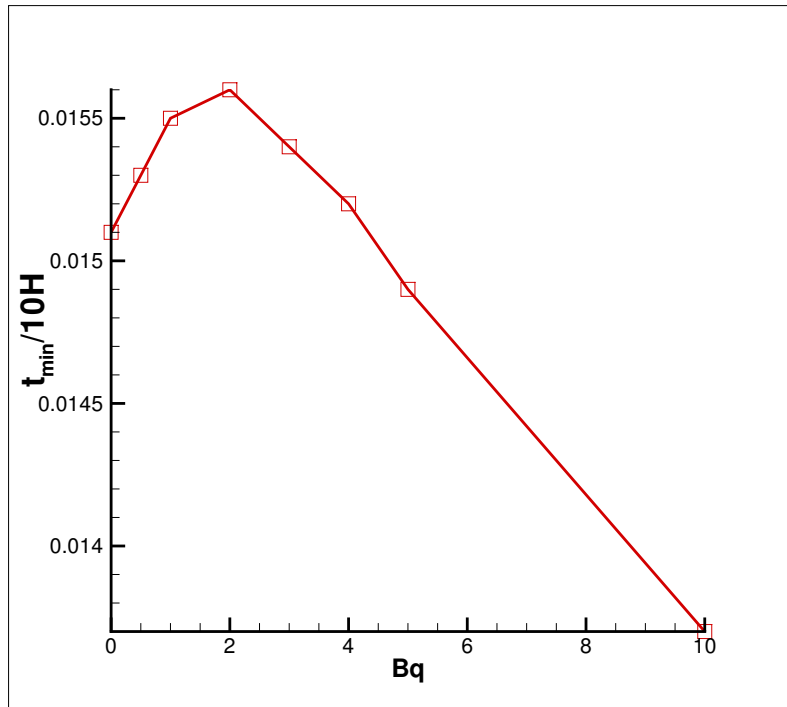
Figure 4.28: The relation between the minimum thickness and the interfacial viscosity for a continuous capillary number equal to 0.2.

viscosity rises, the intensification of this effect drives this recirculation into the cavity. The meniscus follows the recirculation retraction, which causes the angle to decrease with increasing interfacial viscosity. This tendency remains until the influence of viscosity produces another recirculation near the interface separating the two recirculations. For higher values of Boussinesq, the behavior of the angle decreases monotonically.

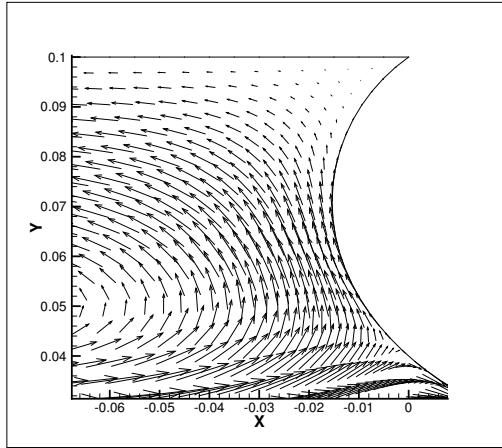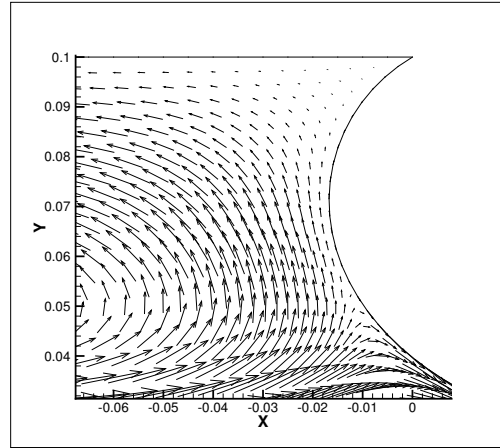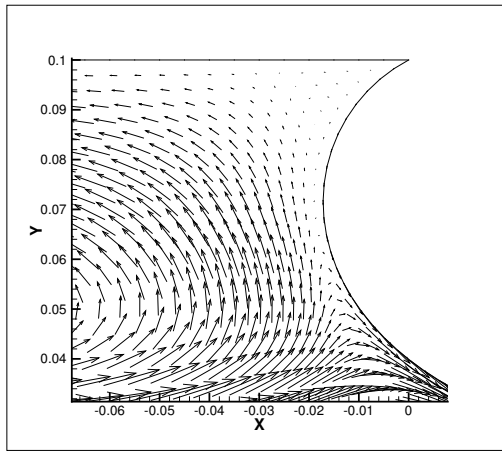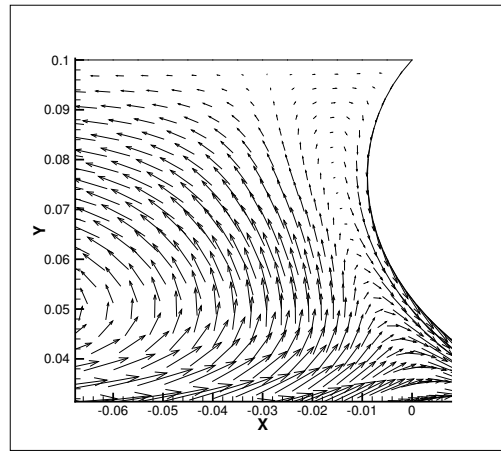4.29(a): Bq = 0

4.29(b): Bq = 0.5

4.29(c): Bq = 1

4.29(d): Bq = 5

Figure 4.29: Velocity profile for the entrance for Ca equals to 0.1 and the dimensionless flow rate equals 0.16. The number of Boussinesq varies between 0, 1, 5 and 10.

These results show that the liquid formulation may be altered in order to achieve a desired surface viscosity, which makes possible coating thinner films.

5
Conclusion

5.1
Final Remarks

A numerical solution based on the Galerkin finite element method enabled the analysis of free surface flow with complex interface. This solution involved the use of the Boussinesq-Scriven model to describe the behavior of viscous free surface. The model was used to study extrusion and slot die coating problems for Newtonian fluids with a viscous interface.

The solution improved the understanding of the effect of interfacial viscosity on extrusion and slot coating flows and showed the strong effect of the interfacial viscosity on the flow behavior. Another conclusion is that capillarity and surface viscosity affect the flow near free surfaces differently. The interfacial tension limits the surface from bending while the viscosity reacts to the surface stretching. So, the effects of interfacial viscosity may not be noticeable by analyzing only the interface displacement.

In the case of extrusion, if the free surface has a viscous behavior, the intensity of the extrudate swell is increased. Moreover, the surface viscosity effect can be more intense than the capillarity in the final film thickness. This effect has a significant influence on the precision of extrudates. The delay in plug flow due to the expansion of the film thickness reduces the extrusion speed.

For the slot coating, the viscous surface increased the development length of the flow, increasing the region of influence of the die. The possibility to reduce the minimum thickness by increasing the surface viscosity allows manufacturing thinner coated layers for a fixed gad between the substrate and the slot lips.

As a conclusion of this work, others research topics arise and might be answered in future works.

5.2
Future works

Naturally, future experimental works should evaluate if these results are consistent, investigating if the retardation of the development flow and its consequences may be attributed to the interface viscosity.

Experiments could be designed with liquids with different surface viscosity to evaluate the effect of interfacial rheology on die swell and minimum thickness in slot coating process.

One important limitation of the model used here is that is does not consider the dynamics of adsorption/desorption of large molecules and particles in the interface. Interface rheology is a function of interface aging time, which is neglected in this work. The inclusion of this important phenomenon will improve the quality of the model.

The elasticity is another interfacial property that can play an essential role in fluid flow. Different interfacial constitutive model could be used to include the effect of surface elasticity.

Bibliography

[1] Martial Sauceau, Jacques Fages, Audrey Common, Clémence Nikitine, and Elisabeth Rodier. New challenges in polymer foaming: A review of extrusion processes assisted by supercritical carbon dioxide. Progress in Polymer Science, 36(6):749–766, 2011.

[2] S Bruin, DJ Van Zuilichem, and W Stolp. A review of fundamental and engineering aspects of extrusion of biopolymers in a single-screw extruder. Journal of Food Process Engineering, 2(1):1–37, 1978.

[3] RJ Koopmans. Die swell or extrudate swell. In Polypropylene, pages 158–162. Springer, 1999.

[4] Kejian Wang. Description of extrudate swell for polymer nanocomposites. Materials, 3(1):386–400, 2010.

[5] OJ Romero and MS Carvalho. Response of slot coating flows to periodic disturbances. Chemical Engineering Science, 63(8):2161–2173, 2008.

[6] OJ Romero, WJ Suszynski, LE Scriven, and MS Carvalho. Low-flow limit in slot coating of dilute solutions of high molecular weight polymer. Journal of Non-Newtonian Fluid Mechanics, 118(2-3):137–156, 2004.

[7] Si Hyung Lee, Hyun Jung Koh, Bo Kyung Ryu, See Jo Kim, Hyun Wook Jung, and Jae Chun Hyun. Operability coating windows and frequency response in slot coating flows from a viscocapillary model. Chemical engineering science, 66(21):4953–4959, 2011.

[8] Marcel Schmitt, Michael Baunach, Lukas Wengeler, Katharina Peters, Pascal Junges, Philip Scharfer, and Wilhelm Schabel. Slot-die processing of lithium-ion battery electrodes—coating window characterization. Chemical Engineering and Processing: Process Intensification, 68:32–37, 2013.

[9] Suk Il Youn, Su Yeon Kim, Dong Myeong Shin, Joo Sung Lee, Hyun Wook Jung, and Jae Chun Hyun. A review on viscocapillary models of pre-metered coating flows. Korea-Australia Rheology Journal, 18(4):209–215, 2006.

[10] Ilhoon Jang and Simon Song. A model for prediction of minimum coating thickness in high speed slot coating. International Journal of Heat and Fluid Flow, 40:180–185, 2013.

[11] Milton J Rosen and Joy T Kunjappu. Surfactants and interfacial phenomena. John Wiley & Sons, 2012.

[12] J. Willard Gibbs. On the equilibrium of heterogeneous substances. Transactions of the Connecticut Academy of Arts and Sciences, 3:108–248, October 1875 – May 1876.

[13] C. Marangoni. Sull'espansione delle goccie d'un liquido galleggianti sulla superfice di altro liquido. Fratelli Fusi, 1865.

[14] Leonard MC Sagis and Peter Fischer. Nonlinear rheology of complex fluid–fluid interfaces. Current opinion in colloid & interface science, 19(6):520–529, 2014.

[15] Serpil Sahin and Servet Gülüm Sumnu. Surface Properties of Foods, pages 229–250. Springer New York, New York, NY, 2006.

[16] Silvia EHJ van Kempen, Henk A Schols, Erik van der Linden, and Leonard MC Sagis. Molecular assembly, interfacial rheology and foaming properties of oligofructose fatty acid esters. Food & function, 5(1):111–122, 2014.

[17] Gerald G Fuller and Jan Vermant. Complex fluid-fluid interfaces: rheology and structure. Annual review of chemical and biomolecular engineering, 3:519–543, 2012.

[18] Jan Pelipenko, Julijana Kristl, Romana Rošic, Saša Baumgartner, and Petra Kocbek. Interfacial rheology: an overview of measuring techniques and its role in dispersions and electrospinning. Acta Pharmaceutica, 62(2):123–140, 2012.

[19] A Gholamipour Shirazi, MS Carvalho, MFG Huila, Koiti Araki, P Dommersnes, and JO Fossum. Transition from glass-to gel-like states in clay at a liquid interface. Scientific Reports, 6:1–8, 2016.

[20] Azarmidokht Gholamipour-Shirazi, Marcio S Carvalho, and Jon Otto Fossum. Controlled microfluidic emulsification of oil in a clay nanofluid: Role of salt for pickering stabilization. The European Physical Journal Special Topics, 225(4):757–765, 2016.

[21] Liat Rosenfeld and Gerald G Fuller. Consequences of interfacial viscoelasticity on thin film stability. Langmuir, 28(40):14238–14244, 2012.

[22] M Saad Bhamla, Caroline E Giacomin, Caroline Balemans, and Gerald G Fuller. Influence of interfacial rheology on drainage from curved surfaces. Soft Matter, 10(36):6917–6925, 2014.

[23] Sven Reynaert, Carlton F Brooks, Paula Moldenaers, Jan Vermant, and Gerald G Fuller. Analysis of the magnetic rod interfacial stress rheometer. Journal of Rheology, 52(1):261–285, 2008.

[24] J Krägel, SR Derkatch, and R Miller. Interfacial shear rheology of protein–surfactant layers. Advances in colloid and interface science, 144(1-2):38–53, 2008.

[25] Philipp Erni. Deformation modes of complex fluid interfaces. Soft Matter, 7(17):7586–7600, 2011.

[26] Alejandro D Rey. Linear viscoelastic model for bending and torsional modes in fluid membranes. Rheologica acta, 47(8):861–871, 2008.

[27] D.J. Acheson. Elementary Fluid Dynamics. Comparative Pathobiology - Studies in the Postmodern Theory of Education. Clarendon Press, 1990.

[28] Arnold Reusken and Yuanjun Zhang. Numerical simulation of incompressible two-phase flows with a boussinesq–scriven interface stress tensor. International journal for numerical methods in fluids, 73(12):1042–1058, 2013.

[29] Joel Romero Guzman Oldrich. Limite de vazão mínima do processo de revestimento por extrusão de soluções poliméricas. 2003.

[30] Rodrigo Bento Reboucas. Shear sensitive particle suspension flows in slot coating. 2016.

[31] Dean F Benjamin. Roll coating flows and multiple roll systems. 1996.

[32] Kostas Nikiforos Christodoulou. Computational physics of slide coating flow. 1990.

[33] KN Christodoulou and LE Scriven. Discretization of free surface flows and other moving boundary problems. Journal of Computational Physics, 99(1):39–55, 1992.

[34] Ivo M Babuska. The finite element method with lagrangian multipliers. Numerische Mathematik, 20(3):179–192, 1973.

[35] Leopoldo P Franca and Sérgio L Frey. Stabilized finite element methods: Ii. the incompressible navier-stokes equations. *Computer Methods in Applied Mechanics and Engineering*, 99(2-3):209–233, 1992.